host cell plasma membrane proteins on the basis of their membrane anchoring. J. Exp. Med. **190:**1783–1792.
18. **Murakami, S., H. Araki, S. Otomo, Y. Nara, and Y. Yamori.** 1995. Effects of HL-004, a novel ACAT inhibitor, on cholesterol accumulation and removal in cultured smooth muscle cell from stroke-prone spontaneously hypertensive rats (SHRSP). Life Sci. **56:**509–520.
19. **Murakami, S., I. Yamagishi, Y. Asami, M. Sato, and K. Tomisawa.** 1996. Effect of the ACAT inhibitor, HL-004, on cholesterol metabolism in macrophages. Cell. Mol. Biol. **42:**865–872.
20. **Nagai, H., J. C. Kagan, X. Zhu, R. A. Kahn, and C. R. Roy.** 2002. A bacterial guanine nucleotide exchange factor activates ARF on *Legionella* phagosomes. Science **295:**679–682.
21. **Naroeni, A., and F. Porte.** 2002. Role of cholesterol and the ganglioside GM_1 in entry and short-term survival of *Brucella suis* in murine macrophages. Infect. Immun. **70:**1640–1644.
22. **Ono, A., and E. O. Freed.** 2001. Plasma membrane rafts play a critical role in HIV-1 assembly and release. Proc. Natl. Acad. Sci. USA **98:**13925–13930.
23. **Pentchev, P. G., M. T. Vanier, K. Suzuki, and M. C. Patterson.** 1995. XVI. Lysosomal disorders, p. 2625–2640. *In* C. R. Scriver, A. L. Beaudet, W. S. Sly, and D. Valle (ed.), The metabolic and molecular basis of inherited disease. McGraw-Hill Inc., New York, N.Y.
24. **Pizarro-Cerda, J., E. Moreno, V. Sanguedolce, J. L. Mege, and J. P. Gorvel.** 1998. Virulent *Brucella abortus* prevents lysosome fusion and is distributed within autophagosome-like compartments. Infect. Immun. **66:**2387–2392.
25. **Sawamura, N., J.-S. Gong, W. S. Garver, R. A. Heidenreich, H. Ninomiya, K. Ohno, K. Yanagisawa, and M. Michikawa.** 2001. Site-specific phosphorylation of Tau accompanied by activation of mitogen-activated protein kinase (MAPK) in brains of Niemann-Pick type C mice. J. Biol. Chem. **276:**10314–10319.
26. **Scheiffele, P., A. Rietveld, T. Wilk, and K. Simons.** 1999. Influenza viruses select ordered lipid domains during budding from the plasma membrane. J. Biol. Chem. **274:**2038–2044.
27. **Sieira, R., D. J. Comerci, D. O. Sanchez, and R. A. Ugalde.** 2000. A homologue of an operon required for DNA transfer in *Agrobacterium tumefaciens* is required in *Brucella abortus* for virulence and intracellular multiplication. J. Bacteriol. **182:**4849–4855.
28. **Simons, K., and G. van Meer.** 1988. Lipid sorting in epithelial cells. Biochemistry. **27:**6197–6202.
29. **Sugimoto, Y. H. Ninomiya, Y. Ohsaki, K. Higaki, J. P. Davies, Y. A. Ioannou, and K. Ohno.** 2001. Accumulation of cholera toxin and GM1 ganglioside in the early endosome of Niemann-Pick C1-deficient cells. Proc. Natl. Acad. Sci. USA **98:**12391–12396.
30. **Swanson, M. S., and R. R. Isberg.** 1996. Identification of *Legionella pneumophila* mutants that have aberrant intracellular fates. Infect. Immun. **64:** 2585–2594.
31. **Watarai, M., I. Derre, J. Kirby, J. D. Growney, W. F. Dietrich, and R. R. Isberg.** 2001. *Legionella pneumophila* is internalized by a macropinocytotic uptake pathway controlled by the Dot/Icm system and the mouse *Lgn1* locus. J. Exp. Med. **194:**1081–1095.
32. **Watarai, M., S.-I. Makino, and T. Shirahata.** 2002. An essential virulence protein of *Brucella abortus*, VirB4, requires an intact nucleoside triphosphate-binding domain. Microbiology **148:**1439–1446.
33. **Watarai, M., S.-I. Makino, Y. Fujii, K. Okamoto, and T. Shirahata.** 2002. Modulation of *Brucella*-induced macropinocytosis by lipid rafts mediates intracellular replication. Cell. Microbiol. **4:**341–355.
34. **Zhang, M., N. K. Dwyer, E. B. Neufeld, D. C. Love, A. Cooney, M. Comly, S. Patel, H. Watari, J. F. Strauss III, P. G. Pentchev, J. A. Hanover, and E. J. Blanchette-Mackie.** 2001. Sterol-modulated glycolipid sorting occurs in Niemann-Pick C1 late endosomes. J. Biol. Chem. **276:**3417–3425.

Editor: D. L. Burns

Niemann-Pick C1 protein regulates cholesterol transport to the *trans*-Golgi network and plasma membrane caveolae

William S. Garver,[1,*] Kumar Krishnan,[*] Jayme R. Gallagos,[*] Makoto Michikawa,[†] Gordon A. Francis,[§] and Randall A. Heidenreich[*]

Department of Pediatrics,[*] Arizona Health Sciences Center, The University of Arizona, 1501 N. Campbell Avenue, Tucson, AZ 85724; Department of Dementia Research,[†] National Institute for Longevity Sciences, 36-3 Gengo, Morioka, Obu, Aichi 474-8522, Japan; and CIHR Group on Molecular and Cell Biology of Lipids and Department of Medicine,[§] University of Alberta, Edmonton, Alberta, Canada, T6G 2S2

Abstract **The Niemann-Pick C1 (NPC1) protein regulates cholesterol transport from late endosomes-lysosomes to other intracellular compartments. In this article, cholesterol transport to caveolin-1 and caveolin-2 containing compartments, such as the *trans*-Golgi network (TGN) and plasma membrane caveolae, was examined in normal ($NPC^{+/+}$), NPC heterozygous ($NPC^{+/-}$), and NPC homozygous ($NPC^{-/-}$) human fibroblasts. The expression and distribution of NPC1 in each cell type were similar, and characterized by a finely dispersed, granular staining pattern. The expression of caveolin-1 and caveolin-2 was increased in $NPC^{+/-}$ and $NPC^{-/-}$ fibroblasts, although the distribution in each cell type was similar and characterized by predominant staining of the TGN and plasma membrane. The TGN in $NPC^{+/+}$ fibroblasts was relatively cholesterol-enriched, whereas the TGN in $NPC^{+/-}$ and $NPC^{-/-}$ fibroblasts was partially or completely cholesterol-deficient, respectively. Consistent with studies demonstrating the transport of cholesterol from the TGN to plasma membrane caveolae, the concentration of cholesterol in plasma membrane caveolae isolated from $NPC^{+/-}$ and $NPC^{-/-}$ fibroblasts was significantly decreased, even though the total concentration of plasma membrane cholesterol in each cell type was similar. These studies demonstrate that NPC1 regulates cholesterol transport to caveolin-1 and caveolin-2 containing compartments such as the TGN and plasma membrane caveolae.**—Garver, W. S., K. Krishnan, J. R. Gallagos, M. Michikawa, G. A. Francis, and R. A. Heidenreich. **Niemann-Pick C1 protein regulates cholesterol transport to the *trans*-Golgi network and plasma membrane caveolae.** ***J. Lipid Res.*** **2002.** 43: **579–589.**

Supplementary key words caveolin-1 • caveolin-2 • fibroblasts

Niemann-Pick type C (NPC) disease is a rare neurodegenerative disorder characterized by the accumulation of cholesterol within most tissues (1, 2). The accumulation of cholesterol in tissues of NPC mice is proportional to the endocytosis of LDL through the clathrin coated-pit pathway (3). At the cellular level, NPC cells accumulate cholesterol in late endosomes-lysosomes and the *trans*-cisternae of the Golgi apparatus, delaying cholesterol transport to other cellular compartments responsible for maintaining cholesterol homeostasis (4–6). Recent results suggest that endogenously synthesized and plasma membrane-derived cholesterol may also contribute to the accumulation of cholesterol in late endosomes-lysosomes of NPC cells, most likely as a result of constitutive plasma membrane internalization through the clathrin coated-pit pathway (7–10).

The human gene responsible for the first complementation group of NPC has been identified and shown to encode the Niemann-Pick C1 (NPC1) protein (11). The NPC1 protein contains several structural motifs that are required to regulate the mobilization of late endosomal-lysosomal cholesterol. Among these are the following: a unique cysteine-rich NPC1 domain that contains a leucine zipper, a sterol-sensing domain homologous to domains in 3-hydroxy-3-methylglutaryl coenzyme A (HMG-CoA) reductase and the sterol-regulatory element binding protein (SREBP) cleavage-activating protein (SCAP), and a carboxy-terminal dileucine motif that mediates endocytosis to late endosomes-lysosomes (12–15). When normal ($NPC^{+/+}$) fibroblasts are incubated in the presence of LDL, the NPC1 protein localizes to a distinct subset of vesicles containing late endosome-lysosome markers, and to a lesser extent, the *trans*-Golgi network (TGN) (16–19). This NPC1-containing compartment is believed to function as a sterol-modulated late endosomal sorting organelle that facilitates the transport of LDL-derived and plasma membrane-derived cholesterol (20, 21). Studies have also demonstrated that particular Rab proteins (Rab7 and Rab9) colocalize with NPC1 and are involved in facilitating the

Abbreviations: MAPK, mitogen-activated protein kinase; NPC1, Niemann-Pick C1 protein; NPC, Niemann-Pick type C; SREBP, sterol-regulatory element binding protein; SCAP, SREBP cleavage-activating protein; TGN, *trans*-Golgi network.

[1] To whom correspondence should be addressed.
e-mail: wgarver@peds.arizona.edu

fission-fusion of vesicles transported between late endosomes-lysosomes and the TGN (18, 20, 22). Recent studies suggest that NPC1 may also function as a sterol-modulated transmembrane efflux pump that uses a proton-motive force to remove lipids, specifically fatty acids, from late endosomes-lysosomes (23).

Previous studies have shown that the expression of caveolin-1 is increased in NPC heterozygous ($NPC^{+/-}$) and NPC homozygous ($NPC^{-/-}$) fibroblasts and tissues (24, 25). Consistent with the hypothesis that increased caveolin-1 expression may participate in a compensatory mechanism involved in the transport of late endosome-lysosome cholesterol, a recent study has demonstrated that a caveolin dominant negative mutant induces intracellular cholesterol imbalance by promoting cholesterol accumulation in late endosomes-lysosomes (26). The treatment of these cells with U18666A, an amphiphile that induces a phenotype similar to NPC, acts synergistically with the caveolin dominant negative mutant to increase the accumulation of cholesterol in late endsomes-lysosomes (26). Both caveolin-1 and caveolin-2 have been shown to be integral membrane proteins of the TGN and TGN-derived vesicles (27–29). Caveolins also serve as coat-proteins for specialized flask-shaped domains of the plasma membrane called caveolae, previously proposed to regulate intracellular cholesterol homeostasis and transmembrane signaling events (30–33). Studies have characterized the caveolins as cholesterol-binding proteins involved in transporting endogenously synthesized cholesterol and LDL-derived cholesterol to plasma membrane caveolae (33–36). In the present report, $NPC^{+/+}$, $NPC^{+/-}$, and $NPC^{-/-}$ human fibroblasts were used to examine the role of NPC1 in regulating cholesterol transport to caveolin-1 and caveolin-2 containing compartments such as the TGN and plasma membrane caveolae.

MATERIALS AND METHODS

Materials

DMEM, PBS, FBS, trypsin-EDTA, and penicillin-streptomycin were purchased from Mediatech (Herndon, VA). Protease inhibitor cocktail tablets were purchased from Boehringer Mannheim (Germany). Antibodies generated against the carboxy-terminus of human NPC1 were generously provided by Peter G. Pentchev (National Institutes of Health, Bethesda, MD) and Shutish Patel (Veterans Administration Connecticut Healthcare System, Newington, CT). Mouse anti-caveolin-1 (clone 2297), rabbit anti-caveolin-1, and mouse anti-caveolin-2 (clone 65) were purchased from BD Biosciences (San Diego, CA). Rabbit anti-N-cadherin was generously provided by Ron L. Heimark (The University of Arizona, Tucson, AZ). Mouse anti-protein disulfide isomerase (PDI) was purchased from Affinity BioReagents (Golden, CO). Peroxidase-conjugated goat secondary antibodies were purchased from Kirkegaard and Perry Laboratories (Gaithersburg, MD). Cy2- and Cy3-conjugated goat secondary antibodies were purchased from Jackson Immunoresearch Laboratories (West Grove, PA). Supersignal substrate for Western blotting, Immunopure IgG elution buffer, and bicinchoninic acid (BCA) protein assay kit were purchased from Pierce-Endogen (Rockford, IL). Nalco 2329 colloidal silica was purchased from Nalco Chemical Company (Chicago, IL). Polyacrylic acid (250,000 Da) was purchased from Polysciences (Warrington, PA). Aluminum chlorohydroxide was purchased from Reheis Incorporated (Berkeley Heights, NJ). Nycodenz, filipin, morpholinoethanesulfonic acid (Mes), and mouse anti-Golgi 58 kDa protein were purchased from Sigma Chemical Company (St. Louis, MO).

Cell culture

$NPC^{+/+}$ fibroblasts (CRL-2076 and CRL-2097) were purchased from American Type Culture Collection (Manassas, VA). Human $NPC^{+/-}$ fibroblasts (H-2325 and H-2327) were generously provided by Wenda L. Greer and David M. Byers (Dalhousie University, Halifax, Nova Scotia, Canada). Human $NPC^{-/-}$ fibroblasts (GM-03123A and GM-11094) were purchased from the Human Genetic Mutant Cell Repository (Camden, NJ). In most experiments conducted in this report, both cell lines from $NPC^{+/+}$, $NPC^{+/-}$, and $NPC^{-/-}$ fibroblasts were used. The reported results are representative of the particular cell type. For all experiments, fibroblasts were grown to near confluence in DMEM containing 10% FBS and 1% penicillin-streptomycin.

Preparation of cationic colloidal silica

Cationic colloidal silica was prepared as previously described (37, 38). This was accomplished by adding 35 gm of the aluminum chlorohydroxide complex (50%, w/w) and 450 gm of Nalco 2329 colloidal silica into 300 ml distilled water and blending for 2 min at high speed. The resulting suspension was incubated in a water bath at 80°C for 30 min and then overnight at room temperature. The mixture was adjusted to pH 5.0 using 1 N NaOH until stable for at least 24 h.

Isolation of plasma membrane and caveolae

The plasma membrane and caveolae were isolated from human fibroblasts using cationic colloidal silica as previously described (37, 38). Fibroblasts were rinsed once with PBS, and then twice with MBS-1 (20 mM Mes, pH 5.5, 135 mM NaCl). The cells were incubated in MBS-1 containing 1.0% cationic colloidal silica for 10 min, and then rinsed once with MBS-1. The cells were incubated in MBS-2 (20 mM Mes, pH 6.0, 135 mM NaCl) containing 1.0 mg/ml polyacrylic acid (250,000 Da) for 10 min, and then rinsed twice with MBS-2. The cells were scraped from the plate using MBS-2 containing a protease inhibitor cocktail and then pelleted using centrifugation (1,000 *g*, 10 min). The cell pellet was resuspended in MBS-3 (10 mM Mes pH 6.5) containing a protease inhibitor cocktail and aspirated using a 23-G needle. The samples were homogenized using a type C Teflon-glass homogenizer and diluted with an equal volume of MBS-4 (10 mM Mes pH 6.5, 270 mM NaCl) containing 100% (w/v) Nycodenz. The resulting 50% Nycodenz mixture was layered on a 70–55% linear Nycodenz gradient prepared in MBS-5 (10 mM Mes pH 6.5, 135 mM NaCl) and centrifuged (60,000 *g* for 30 min) using a Beckman SW-40 Ti rotor. After centrifugation, the purified cationic colloidal silica-coated plasma membrane was recovered and rinsed twice with MBS-5. The plasma membrane was extracted using MBS-6 (20 mM Mes pH 6.0, 135 mM NaCl) containing 1.0% Triton X-100 and homogenized using a type AA Teflon-glass homogenizer. An equal volume of 40 mM KCl containing 80% sucrose was added to the resulting homogenate and overlayed with a discontinuous sucrose step gradient (1 ml each of 35%, 30%, 25%, 20%, 15%, 10%, 5%, and 0% sucrose dissolved in 20 mM KCl). The sample was centrifuged (85,000 *g* for 16 h) using a Beckman SW-40 Ti rotor. The resulting opalescent band present at the 10–15% sucrose interface representing purified caveolae was collected and concentrated using centricon-10 concentrators.

Determination of cholesterol concentration

To determine cholesterol concentration, samples were extracted with hexane-isopropanol (3:2, v/v) and the lipids were separated using conventional thin-layer chromatography with hexane-diethyl ether-glacial acetic acid (80:20:1, v/v/v). Cholesterol was identified by comigration using a cholesterol standard after staining plates with iodine vapors. Spots representing cholesterol were scraped from the plate and extracted with hexane-water (3:1, v/v). After evaporation of the hexane phase, the mass of cholesterol was determined using the cholesterol oxidase method (39).

Determination of caveolae cholesterol

The amount of caveolae cholesterol was determined by labeling fibroblasts with [^{3}H]cholesterol and incubating with cholesterol oxidase (33). Cholesterol oxidase specifically oxidizes plasma membrane caveolae cholesterol to cholestenone, where both separated using thin-layer chromatography. To perform this experiment, fibroblasts were seeded into 6-well plates and grown to approximately 50% confluence in DMEM-10% FBS. Cells were refed with media containing [^{3}H]cholesterol (5.0 μCi/ml) and grown to near confluence (approximately 3 days). Cells were rinsed three times with PBS (37°C) and allowed to equilibrate for 24 h in media. Finally, the cells were incubated in either media alone, or media containing cholesterol oxidase (0.5 U/ml) for 1 h at 37°C. Cells were rinsed three times with PBS and the lipids were extracted to separate [^{3}H]cholesterol and [^{3}H]cholestenone using thin-layer chromatography. The amount of [^{3}H]cholesterol and [^{3}H]cholestenone was determined using liquid scintillation counting.

Immunoblot analysis

Protein samples were separated using 6% or 12% SDS-PAGE under reducing conditions and transferred to a nitrocellulose membrane. Immunoblot buffer (10 mM sodium phosphate, pH 7.4, 150 mM NaCl, 0.05% Tween 20, and 5% non-fat dry milk) was used to block nonspecific sites for 2 h. Immunoblots were incubated overnight at 4°C with respective primary antibodies and then rinsed with PBS (3 × 10 min). The appropriate peroxidase-conjugated goat secondary antibodies were incubated at room temperature for 1 h and then rinsed with PBS (3 × 10 min). Enhanced chemiluminescence (ECL) was performed and images were obtained using film.

Immunofluorescence labeling

Cells were fixed for 30 min using PBS containing 3% paraformaldehyde. Cells were rinsed with PBS (3 × 5 min) and quenched with PBS containing 50 mM NH_4Cl (15 min). Cells were rinsed with PBS (3 × 5 min) and then blocked for 1 h with either PBS containing 10% goat serum and 0.05% saponin, or PBS containing 10% goat serum and 50 μg/ml filipin. Coverslips were incubated for 1 h with primary antibodies. After rinsing with PBS (3 × 5 min), coverslips were incubated for 1 h with the appropriate Cy2- and Cy3-conjugated goat secondary antibodies. Finally, the coverslips were rinsed with PBS (3 × 5 min) and mounted onto slides with Moviol.

Confocal microscopy

Fluorescent images were obtained using a BioRad MCR-1024 ES laser scanning confocal microscope equipped with a Nikon 60X, NA 1.4 oil immersion objective (W. M. Keck Foundation Bioimaging Core Facility, Steele Memorial Children's Research Center, Arizona Health Sciences Center). Simultaneous two-channel recording was performed using excitation wavelengths of 488 and 568 nm, with fluorescein/Cy2 and Cy3 emission filters (522 DF 35 and HQ 598 40). All images were derived from a single optical section estimated to be 1 μm thick. For merged images, the separate Cy2 and Cy3 images were adjusted to similar intensities and then merged using Adobe Photoshop 6.0.

Statistical analysis

Quantitative data is represented as the mean ± SD of four plates. Significant differences ($P \leq 0.05$) between groups of data were determined using the two-tailed Student's *t*-test assuming equal variance.

RESULTS

Relative expression of NPC1, caveolin-1, and caveolin-2

The relative expression of NPC1, caveolin-1, and caveolin-2 was determined in NPC$^{+/+}$, NPC$^{+/-}$, and NPC$^{-/-}$ fibroblasts using immunoblot analysis (**Fig. 1**). The results indicated that in each cell type the relative expression of NPC1 was similar and represented by a band that migrated to approximately 180 kDa. In contrast, the relative expression of caveolin-1 and caveolin-2 in NPC$^{+/-}$ and NPC$^{-/-}$ fibroblasts was increased compared with that in NPC$^{+/+}$ fibroblasts. This result is consistent with a previous report demonstrating that the relative expression of caveolin-1 was significantly increased in several NPC$^{+/-}$ and NPC$^{-/-}$ fibroblast cell lines when compared with NPC$^{+/+}$ fibroblasts (24). Using β-actin as a control, equivalent amounts of homogenate protein were determined to be analyzed. These results demonstrate that although the relative expression of NPC1 is similar in each cell type, the relative expression of both caveolin-1 and caveolin-2 is increased in NPC$^{+/-}$ and NPC$^{-/-}$ fibroblasts.

Association of NPC1, caveolin-1, and caveolin-2 with the plasma membrane and plasma membrane caveolae

To investigate the association of NPC1, caveolin-1, and caveolin-2 with the plasma membrane and plasma mem-

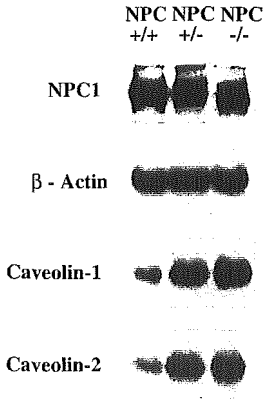

Fig. 1. Relative expression of Niemann-Pick C1 protein (NPC1), caveolin-1, and caveolin-2. Normal NPC$^{+/+}$, NPC heterozygous (NPC$^{+/-}$), and NPC homozygous (NPC$^{-/-}$) fibroblasts were plated and grown to near confluence in DMEM-10% FBS. Cell homogenates were prepared and an equivalent amount of protein (10 μg) from each cell type was used to conduct immunoblot analysis. The immunoblots were reprobed for β-actin to assure that an equivalent amount of protein from each cell type was analyzed. Protein bands were visualized using enhanced chemiluminescence (ECL) and the resulting images were obtained using film.

brane caveolae, the plasma membrane and plasma membrane caveolae were isolated from NPC$^{+/+}$, NPC$^{+/-}$, and NPC$^{-/-}$ fibroblasts using cationic colloidal silica and examined using immunoblot analysis (**Fig. 2**). The sequential purification of the plasma membrane and plasma membrane caveolae in each cell type was monitored using organelle markers. These organelle markers included: β-actin, a cytoskeletal protein present in the cytoplasm and partially associated with the plasma membrane (40); N-cadherin, a plasma membrane cell-adhesion protein (41); the Golgi 58 kDa protein, a protein associated with the TGN (42); and protein disulfide isomerase (PDI), a protein in the endoplasmic reticulum and partially associated with the plasma membrane (43, 44). Caveolin-1 and caveolin-2 were used as markers for plasma membrane caveolae, although both proteins are also associated with the TGN and TGN-derived vesicles (28–30, 45).

The results indicated that β-actin and PDI were detected only in the homogenate and partially with the plasma membrane, but not plasma membrane caveolae. N-cadherin was enriched in the plasma membrane, but absent from plasma membrane caveolae. The Golgi 58 kDa protein was present in the homogenate, but absent

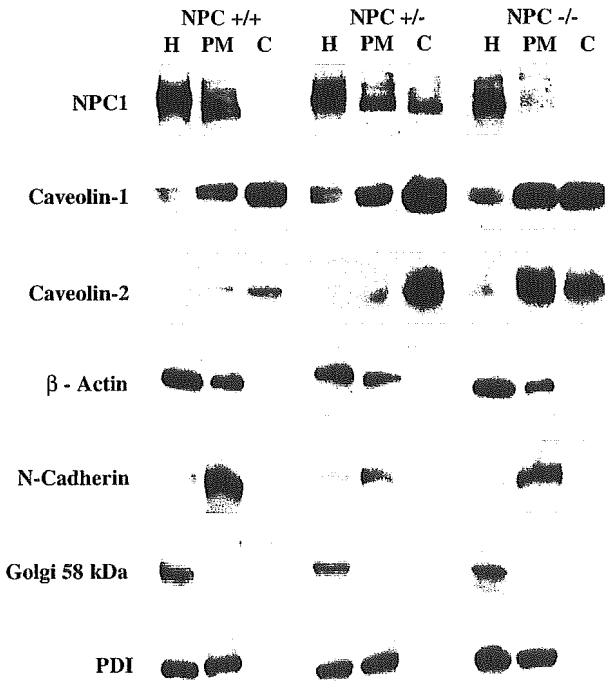

Fig. 2. Association of NPC1, caveolin-1, and caveolin-2 with the plasma membrane and plasma membrane caveolae. NPC$^{+/+}$, NPC$^{+/-}$, and NPC$^{-/-}$ fibroblasts were plated and grown to near confluence in DMEM-10% FBS. Cells were treated with cationic colloidal silica and polyacrylic acid to isolate the plasma membrane using Nycodenz density gradient centrifugation. Plasma membrane caveolae were isolated from the plasma membrane using detergent insoluble sucrose density gradient centrifugation. An equivalent amount of protein (10 μg) from the homogenate (H), plasma membrane (PM), and plasma membrane caveolae (C) from each cell type was used to conduct immunoblot analysis. Protein bands were visualized using ECL and the resulting images were obtained using film.

from the plasma membrane and plasma membrane caveolae. This last result was especially important to demonstrate that plasma membrane caveolae had been successfully isolated using cationic colloidal silica, because it assured that other caveolin-1 and caveolin-2 containing detergent-insoluble membranes commonly associated with the TGN were not contaminating plasma membrane caveolae. With respect to plasma membrane caveolae, the only markers found enriched in this organelle were caveolin-1 and caveolin-2. Consistent with previous reports using cationic colloidal silica to isolate the plasma membrane and plasma membrane caveolae, there was an increasing enrichment of caveolin-1 and caveolin-2 in these compartments (40, 46). However, in contrast with NPC$^{+/+}$ and NPC$^{+/-}$ fibroblasts, in NPC$^{-/-}$ fibroblasts there was a relatively larger amount of caveolin-1 and caveolin-2 associated with the plasma membrane, and not necessarily plasma membrane caveolae. With respect to the distribution of NPC1, results indicated that a fraction of NPC1 was associated with the plasma membrane in each cell type. Interestingly, in NPC$^{+/-}$ fibroblasts, some of the plasma membrane-associated NPC1 resided with plasma membrane caveolae. The association of NPC1 with the plasma membrane in each cell type was confirmed by conducting biotinylation experiments using a membrane-impermeable biotinylating reagent and selective precipitation with streptavidin-conjugated agarose beads (results not shown).

The amount of protein recovered after isolation of the plasma membrane and plasma membrane caveolae in NPC$^{+/+}$, NPC$^{+/-}$, and NPC$^{-/-}$ fibroblasts was also determined (**Table 1**). The results indicated that in NPC$^{+/+}$ fibroblasts 2.18% of the homogenate protein was recovered in the plasma membrane, whereas in NPC$^{+/-}$ and NPC$^{-/-}$ fibroblasts, the amount of homogenate protein recovered in the plasma membrane was 3.79% and 3.43%, respectively. As a result of isolating plasma membrane caveolae, the amount of plasma membrane caveolae protein recovered from the plasma membrane of NPC$^{+/+}$ fibroblasts was 4.33%, whereas the amount of plasma membrane ca-

TABLE 1. The amount of protein recovered after isolation of the plasma membrane and plasma membrane caveolae from NPC$^{+/+}$, NPC$^{+/-}$, and NPC$^{-/-}$ fibroblasts

Fibroblast Genotype	Homogenate	Plasma Membrane	Recovery	Caveolae	Recovery
	mg	*mg*	%	*mg*	%
NPC$^{+/+}$	41.20 ± 7.20	0.90 ± 0.06	2.18	0.039 ± 0.007	4.33
NPC$^{+/-}$	45.60 ± 6.40	1.73 ± 0.20	3.79	0.042 ± 0.012	2.43
NPC$^{-/-}$	74.80 ± 4.00	2.57 ± 0.20	3.43	0.039 ± 0.002	1.52

NPC$^{+/+}$ and NPC$^{+/-}$ fibroblasts were plated into 15 150 mm plates and grown to near confluence in DMEM-10% FBS. NPC$^{-/-}$ fibroblasts were plated into twice as many plates (30 150 mm plates) and grown to near confluence in the same media. The plasma membrane from each cell type was isolated using cationic colloidal silica and Nycodenz density gradient centrifugation. The plasma membrane caveolae from each cell type was isolated from the plasma membrane using detergent insoluble sucrose density gradient centrifugation. The protein obtained from each sample was determined in triplicate using the BCA protein method and the results are reported as the mean ± SD.

veolae protein recovered from the plasma membrane of NPC$^{+/-}$ and NPC$^{-/-}$ fibroblasts was 2.43% and 1.52%, respectively. Because the isolation of plasma membrane caveolae using cationic colloidal silica is dependent on the sheering of these invaginated organelles from the plasma membrane, the decreasing amounts of plasma membrane caveolae protein recovered from NPC$^{+/-}$ and NPC$^{-/-}$ fibroblasts suggests that fewer of these organelles may have initially existed on the cell surface.

Cholesterol concentration of the plasma membrane and plasma membrane caveolae

The amount of cellular, plasma membrane, and plasma membrane caveolae cholesterol was determined in NPC$^{+/+}$, NPC$^{+/-}$, and NPC$^{-/-}$ fibroblasts (**Fig. 3**). As predicted, the concentration of cellular cholesterol in NPC$^{+/-}$ and NPC$^{-/-}$ fibroblasts was significantly increased compared with that of NPC$^{+/+}$ fibroblasts, as previously described (47). Determination of the plasma membrane cholesterol concentration indicated there was no significant difference among the different cell types. This result is consistent with a previous report indicating that the concentration of plasma membrane cholesterol is similar between NPC$^{+/+}$ and NPC$^{-/-}$ fibroblasts (48). However, the concentration of cholesterol measured in plasma membrane caveolae isolated from NPC$^{+/-}$ and NPC$^{-/-}$ fibroblasts was significantly decreased. The concentration of cholesterol measured in plasma membrane caveolae isolated from NPC$^{+/-}$ and NPC$^{-/-}$ fibroblasts was only 30–35% compared with the concentration of cholesterol measured in plasma membrane caveolae isolated from NPC$^{+/+}$ fibroblasts. There was no significant difference in the concentration of cholesterol measured in plasma membrane caveolae between NPC$^{+/-}$ and NPC$^{-/-}$ fibroblasts. To verify these results, an independent method was conducted using cholesterol oxidase to specifically oxidize plasma membrane caveolae cholesterol. The results again indicated that the amount of cholesterol in plasma membrane caveolae from NPC$^{+/-}$ and NPC$^{-/-}$ fibroblasts was only 25–30% of that measured in plasma membrane caveolae from NPC$^{+/+}$ fibroblasts. There was no significant difference in the amount of cholesterol measured in plasma membrane caveolae between NPC$^{+/-}$ and NPC$^{-/-}$ fibroblasts. With respect to the concentration of cholesterol associated with the plasma membrane and plasma membrane caveolae in NPC$^{+/+}$ fibroblasts, it is important to emphasize that the values obtained using cationic colloidal silica was of similar magnitude and concentration as previously reported using independent techniques to isolate these cellular organelles (49, 50). Moreover, the relative concentration of cholesterol associated with plasma membrane caveolae that was measured in the different cell types were of similar magnitude using cholesterol oxidase, an independent method that specifically oxidizes plasma membrane caveolae cholesterol in unfixed cells (32).

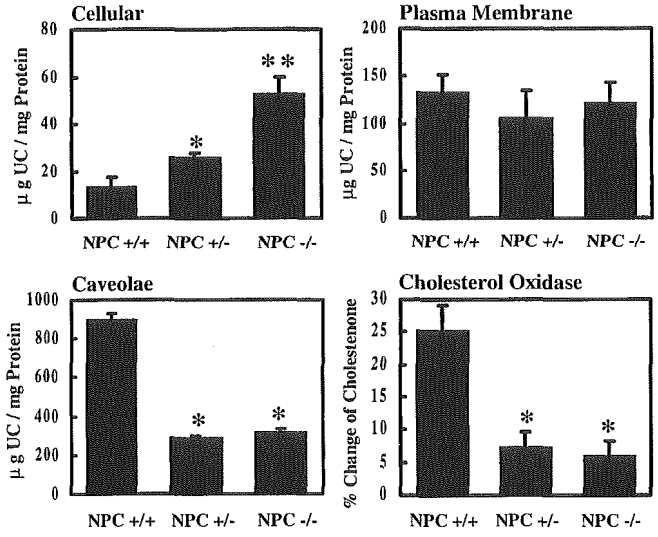

Fig. 3. Cholesterol concentration of the plasma membrane and plasma membrane caveolae. NPC$^{+/+}$, NPC$^{+/-}$, and NPC$^{-/-}$ fibroblasts were plated and grown to near confluence in DMEM-10% FBS. Cells were treated with cationic colloidal silica and polyacrylic acid to isolate the plasma membrane using Nycodenz density gradient centrifugation. Plasma membrane caveolae were isolated from the plasma membrane using detergent insoluble sucrose density gradient centrifugation. To determine the concentration of cholesterol associated with the homogenate, plasma membrane, and plasma membrane caveolae, an equivalent amount of protein (10 μg) from each cell type was analyzed. To determine the amount of cholesterol accessible to cholesterol oxidase, fibroblasts were plated and grown to near confluence in DMEM-10% FBS and labeled with [^{3}H]cholesterol for 24 h. After rinsing with PBS, the cells were incubated with cholesterol oxidase for 1 h at 37°C to convert caveolae [^{3}H]cholesterol to [^{3}H]cholestenone. For each experiment, the values represent the mean ± SD cholesterol concentration (μg UC/mg protein) or the mean ± SD percent change of cholestenone (% change) from three plates. An asterisk represents a significant difference ($P \leq 0.05$) compared with NPC$^{+/+}$. Two asterisks represents a significant difference ($P \leq 0.05$) between NPC$^{+/+}$ and NPC$^{+/-}$.

Fluorescence microscopy of caveolin-1, caveolin-2, and the Golgi 58 kDa protein

The cellular distribution of caveolin-1, caveolin-2, and the Golgi 58 kDa protein was examined in NPC$^{+/+}$, NPC$^{+/-}$, and NPC$^{-/-}$ fibroblasts using double-label fluorescence confocal microscopy (**Fig. 4**). The results indicated that in each cell type caveolin-1 and caveolin-2 (Fig. 4, left column) primarily colocalized with the Golgi 58 kDa protein (Fig. 4, middle column), as evident in the merged images (Fig. 4, right column). However, in each cell type there were additional caveolin-1 and caveolin-2 containing vesicles present in the cytoplasm that did not colocalize with the Golgi 58 kDa protein. Presumably, these additional caveolin-1 and caveolin-2 containing vesicles represented either TGN-derived vesicles or other cytoplasmic transport vesicles as previously described (28, 51).

Fluorescence microscopy of caveolin-1, caveolin-2, and PDI

The cellular distribution of caveolin-1, caveolin-2, and PDI were examined in NPC$^{+/+}$, NPC$^{+/-}$, and NPC$^{-/-}$ fibroblasts using double-label fluorescence confocal mi-

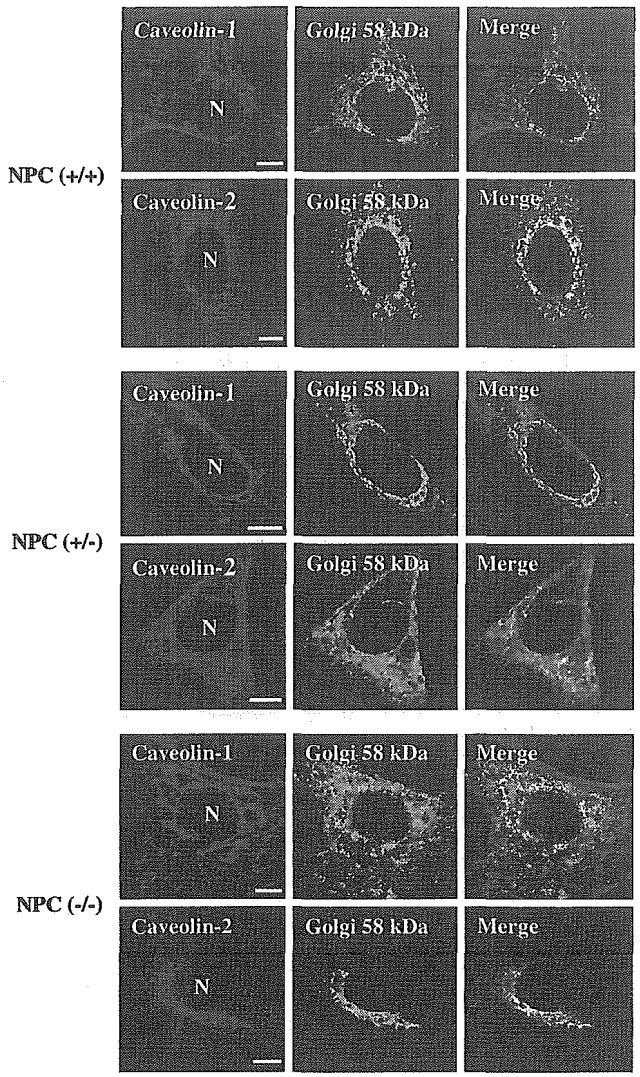

Fig. 4. Fluorescence microscopy of caveolin-1, caveolin-2, and the Golgi 58 kDa protein. $NPC^{+/+}$, $NPC^{+/-}$, and $NPC^{-/-}$ fibroblasts were plated onto coverslips and grown to near confluence in DMEM-10% FBS. The fibroblasts were stained for either caveolin-1 or caveolin-2 (left column), and the Golgi 58 kDa protein (middle column). Images were obtained for each cell type using double-label fluorescence confocal microscopy. For each cell type a merged image is provided (right column). The images were obtained using a single confocal section. N, nucleus. The bar represents 5 μm.

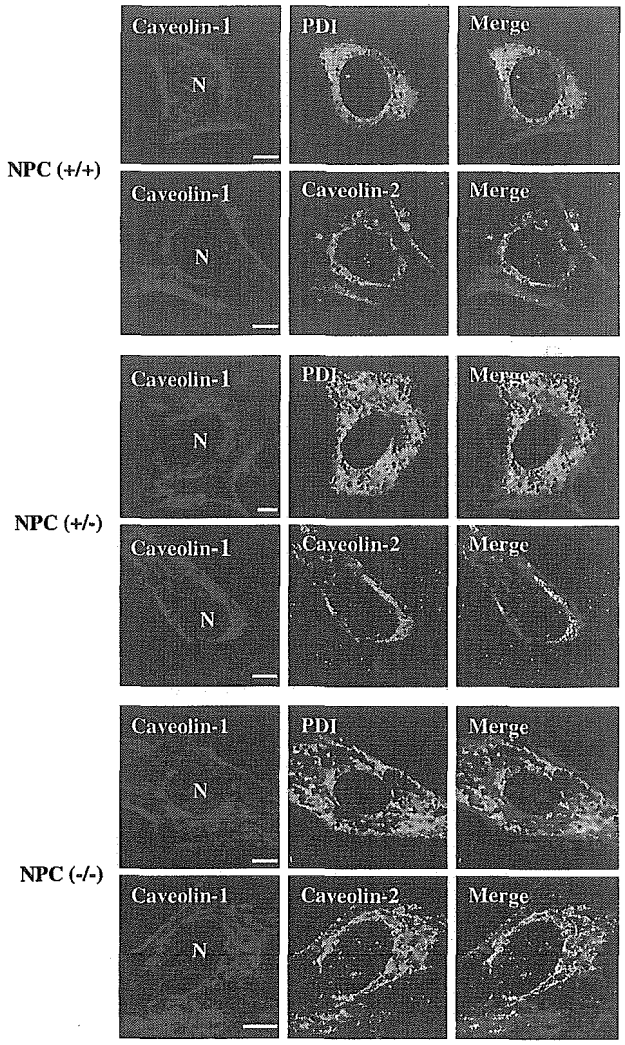

Fig. 5. Fluorescence microscopy of caveolin-1, caveolin-2, and PDI. $NPC^{+/+}$, $NPC^{+/-}$, and $NPC^{-/-}$ fibroblasts were plated onto coverslips and grown to near confluence in DMEM-10% FBS. The fibroblasts were stained for caveolin-1 (left column), and either caveolin-2 or the Golgi 58 kDa protein (middle column). Images were obtained for each cell type using double-label fluorescence confocal microscopy. For each cell type a merged image is provided (right column). The images were obtained using a single confocal section. N, nucleus. The bar represents 5 μm.

croscopy (**Fig. 5**). The results indicated that in each cell type caveolin-1 (Fig. 5, left column) did not colocalize with PDI (Fig. 5, middle column), as evident in the merged images (Fig. 5, right column). This result is consistent with two previous studies indicating that the amount of endogenous caveolin-1 associated with the endoplasmic reticulum is relatively small (26, 52). The finding that increased expression of caveolin-1 in $NPC^{+/-}$ and $NPC^{-/-}$ fibroblasts did not promote colocalization with the endoplasmic reticulum marker suggested that increased caveolin-1 expression may be due to NPC1 deficiency, and not to changes in the trafficking of caveolin-1 due to overexpression. The results also indicate that in each cell type caveolin-1 (Fig. 5, left column) and caveolin-2 (Fig. 5, middle column) colocalize at the TGN, as evident in the merged images (Fig. 5, right column). These results are consistent with the colocalization of caveolin-1 and caveolin-2 at the TGN and TGN-derived vesicles as previously described (28, 45, 51).

Fluorescence microscopy of NPC1, caveolin-1, and caveolin-2

The cellular distribution of NPC1, caveolin-1, and caveolin-2 was examined in $NPC^{+/+}$, $NPC^{+/-}$, and $NPC^{-/-}$ fibroblasts using double-label fluorescence confocal microscopy (**Fig. 6**). The results indicated that in each cell type the cellular distribution of NPC1 was similar and represented by a finely dispersed granular staining pattern within the perinuclear region (Fig. 6, left column). The distribution of caveolin-1 and caveolin-2 in each cell type was similar and primarily represented by staining of the

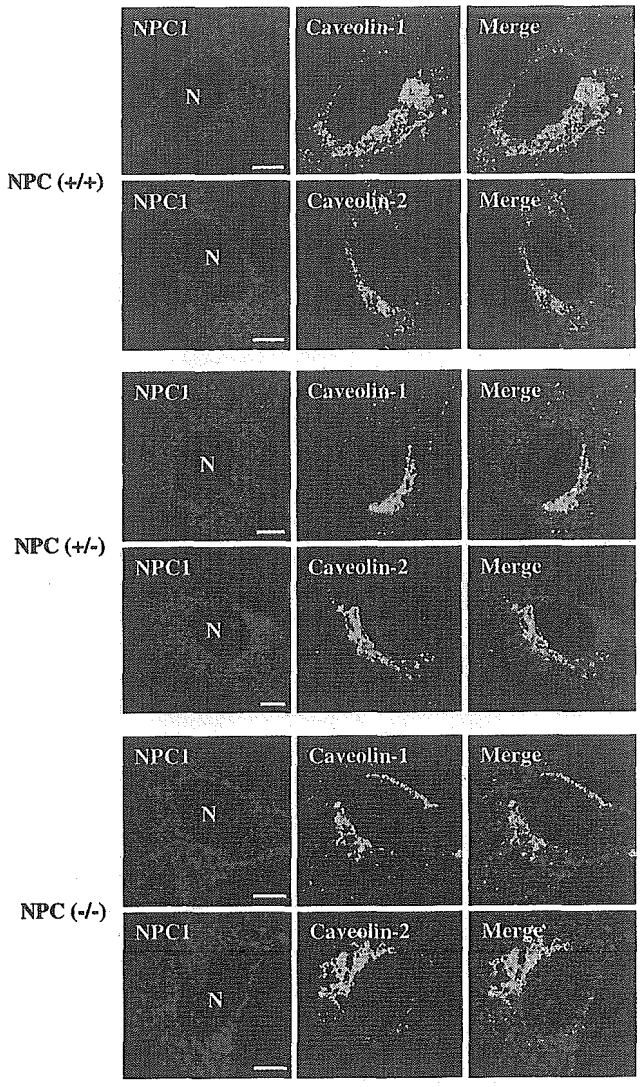

Fig. 6. Fluorescence microscopy of NPC1, caveolin-1, and caveolin-2. NPC$^{+/+}$, NPC$^{+/-}$, and NPC$^{-/-}$ fibroblasts were plated onto coverslips and grown to near confluence in DMEM-10% FBS. The fibroblasts were stained for NPC1 (left column), and either caveolin-1 or caveolin-2 (middle column). Images were obtained for each cell type using double-label fluorescence confocal microscopy. For each cell type a merged image is provided (right column). The images were obtained using a single confocal section. N, nucleus. The bar represents 5 μm.

TGN and other caveolin-1 and caveolin-2 containing vesicles within the cytoplasm (Fig. 6, middle column). There was no extensive colocalization of NPC1 with either caveolin-1 and caveolin-2 at the TGN, or other caveolin-1 and caveolin-2 containing vesicles in the cytoplasm (Fig. 6, right column). This result is somewhat contradictory to previous studies describing partial colocalization of NPC1 with the TGN and caveolin-1 containing vesicles, but reconciled when considering that murine fibroblasts contain two distinct populations of NPC1 (18, 19). The larger of the two NPC1-containing vesicles in murine fibroblasts, which is apparently not detected in human fibroblasts, contains caveolin-1 and has an extensive network of internal membranes (19).

Fluorescence microscopy of caveolin-1, caveolin-2, and filipin

The cellular distribution of caveolin-1, caveolin-2, and filipin was examined in NPC$^{+/+}$, NPC$^{+/-}$, and NPC$^{-/-}$ fibroblasts using double-label fluorescence confocal microscopy (**Fig. 7**). The results indicated that in NPC$^{+/+}$ fibroblasts the caveolin-1 and caveolin-2 containing TGN (Fig. 7, left column) colocalized with filipin (Fig. 7, middle column), as evident in the merged image (Fig. 7, right column). This suggested that in NPC$^{+/+}$ fibroblasts the TGN was relatively cholesterol-enriched, as previously described (5). However, in NPC$^{+/-}$ fibroblasts, the caveolin-1 and caveolin-2 containing TGN (Fig. 7, left column) only partially colocalized with filipin (Fig. 7, middle column), as evident in the merged image (Fig. 7, right column),

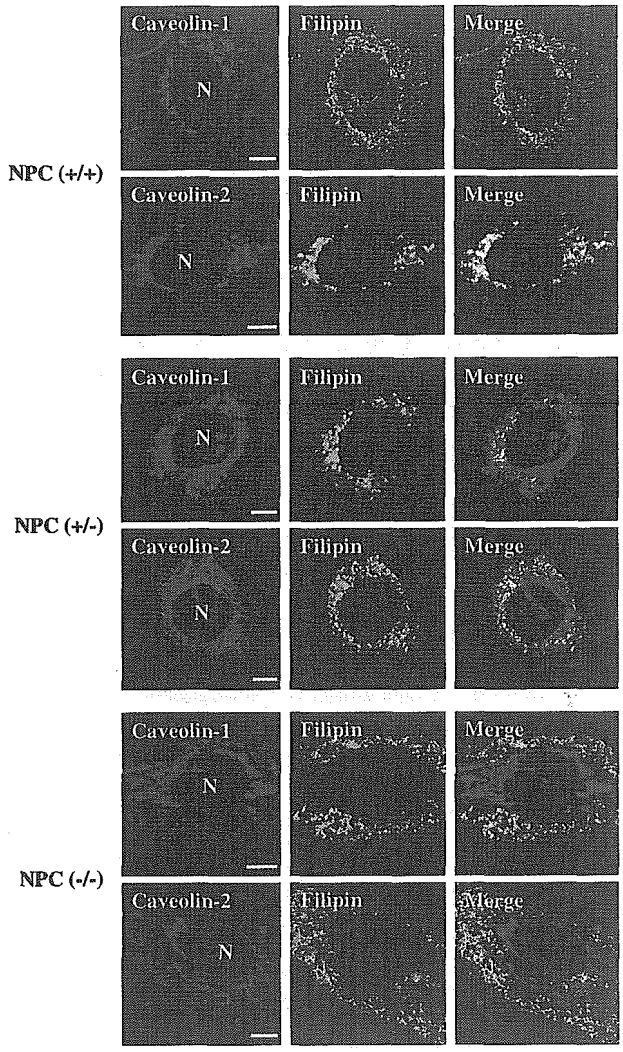

Fig. 7. Fluorescence microscopy of caveolin-1, caveolin-2, and filipin. NPC$^{+/+}$, NPC$^{+/-}$, and NPC$^{-/-}$ fibroblasts were plated onto coverslips and grown to near confluence in DMEM-10% FBS. The fibroblasts were stained for either caveolin-1 or caveolin-2 (left column), and cholesterol using filipin (middle column). Images were obtained for each cell type using double-label fluorescence confocal microscopy. For each cell type a merged image is provided (right column). The images were obtained using a single confocal section. N, nucleus. The bar represents 5 μm.

suggesting that the TGN was partially cholesterol-deficient. Finally, in $NPC^{-/-}$ fibroblasts, the caveolin-1 and caveolin-2 containing TGN (Fig. 7, left column) did not colocalize with filipin (Fig. 7, middle column), suggesting that the TGN was cholesterol-deficient and that a complete defect in the transport of cholesterol to the TGN was present in these cells.

DISCUSSION

The cholesterol transport pathway regulated by NPC1 is a subject of intense investigation. Previous studies suggest that NPC1 regulates cholesterol transport from late endosomes-lysosomes to the plasma membrane (4, 53, 54). The majority of this cholesterol is believed to flow through elements of the Golgi apparatus enroute to the plasma membrane, while the remaining cholesterol is transported to the endoplasmic reticulum in a pathway that is independent of the plasma membrane (55, 56). In contrast, other studies suggest that NPC1 regulates cholesterol transport only after reaching the plasma membrane (7–9). To further characterize the cholesterol transport pathway that is regulated by NPC1, $NPC^{+/+}$, $NPC^{+/-}$, and $NPC^{-/-}$ human fibroblasts were used to examine cholesterol transport to caveolin-1 and caveolin-2 containing compartments such as the TGN and plasma membrane caveolae. First, the results indicated an increased expression of caveolin-1 and caveolin-2 in $NPC^{+/-}$ and $NPC^{-/-}$ fibroblasts, suggesting involvement of caveolin-1 and caveolin-2 containing compartments in the cholesterol transport defect. Second, compared with the accumulation of cellular cholesterol in $NPC^{+/-}$ and $NPC^{-/-}$ fibroblasts, there was an inverse amount of cholesterol associated with the caveolin-1 and caveolin-2 containing TGN. Third, the concentration of cholesterol associated with plasma membrane caveolae and accessible to cholesterol oxidase was significantly decreased in $NPC^{+/-}$ and $NPC^{-/-}$ fibroblasts.

Previous studies have described the increased expression of caveolin-1 mRNA and caveolin-1 protein in $NPC^{+/-}$ and $NPC^{-/-}$ fibroblasts (24). This same result has also been described in vivo using livers from $NPC^{+/-}$ and $NPC^{-/-}$ mice (25, 57). Consistent with the finding that $NPC^{+/-}$ and $NPC^{-/-}$ fibroblasts accumulate cholesterol, studies have shown that when cells are incubated in the presence of LDL, the amount of caveolin-1 mRNA and caveolin-1 protein increases (58, 59). The molecular mechanism responsible for increased expression of caveolin-1 mRNA and caveolin-1 protein has been shown to involve the SREBP-1 (60). The processing of SREBP-1 is mediated by SCAP, which is activated when the amount of cellular cholesterol decreases (61, 62). This being true, it may be assumed that a defect in the function of NPC1 would prevent cholesterol transport and thereby induce SCAP-mediated processing of SREBP-1 to cause decreased expression of caveolin-1. However, since the expression of caveolin-1 and caveolin-2 is increased in $NPC^{+/-}$ and $NPC^{-/-}$ fibroblasts, there must be an additional mechanism that accounts for the increased expression of these proteins.

The Golgi apparatus is a complex organelle consisting of discrete stacks of cisternae (*cis*, *medial*, and *trans*) and a *trans*-Golgi network having a heterogeneous distribution of cholesterol (63, 64). A number of studies have suggested that the Golgi apparatus has an important role in regulating intracellular cholesterol homeostasis. For instance, the Golgi apparatus contributes to the transport of endogenously synthesized cholesterol enroute to the plasma membrane (65). Other studies indicate that the Golgi apparatus is involved in apolipoprotein-mediated cholesterol efflux (66, 67). With respect to the transport of LDL-derived cholesterol, it has been shown that $NPC^{+/+}$ fibroblasts incubated with LDL accumulate cholesterol in the *cis-medial*-Golgi cisternae and TGN, whereas $NPC^{-/-}$ fibroblasts accumulate cholesterol in the *trans*-Golgi cisternae with the TGN remaining relatively cholesterol-deficient (5, 6). Finally, recent studies indicate that LDL-derived cholesterol is transported from clathrin-coated vesicles into intermediate density vesicles that contain markers for the TGN before reaching plasma membrane caveolae (35).

Consistent with other studies demonstrating that the TGN in $NPC^{+/+}$ fibroblasts is relatively cholesterol-enriched, fluorescence microscopy of caveolin-1 and caveolin-2 with filipin indicated that the TGN colocalized with filipin (5, 63, 64). In contrast, the TGN in $NPC^{+/-}$ fibroblasts only partially colocalized with filipin. This apparent disparity was further evident in $NPC^{-/-}$ fibroblasts, which had no apparent colocalization of filipin with the TGN, suggesting that the TGN was cholesterol-deficient. It has recently been reported that cholesterol is required for the formation and regulated budding of TGN-derived vesicles, and that the formation of lipid rafts critically depends on the level of cholesterol residing within these membranes (68, 69). Indeed, it is well established that caveolin-1 and caveolin-2 serve as major components of the TGN that are responsible for facilitating protein and lipid transport to plasma membrane caveolae (28–30, 51). It is also within the TGN that sphingolipid and cholesterol-enriched rafts are generated for the transport of specific proteins and lipids to the cell surface (29, 70). The inability of cholesterol to gain access to the TGN, as evident in $NPC^{+/-}$ and $NPC^{-/-}$ fibroblasts, may therefore prevent the transport of cholesterol to plasma membrane caveolae, resulting in cholesterol-deficient caveolae.

A decrease in plasma membrane caveolae cholesterol may have adverse effects on cellular function since studies have demonstrated that plasma membrane caveolae participate in various signal transduction events (50, 71). With respect to NPC disease, results suggest that hyperactivation of mitogen-activated protein kinase (MAPK) in brains of $NPC^{-/-}$ mice may contribute to neurodegeneration in NPC disease (72). The specific hyperactivation of MAPK has also been shown to occur in $NPC^{-/-}$ fibroblasts (unpublished results). The inability to demonstrate MAPK hyperactivation in $NPC^{+/-}$ fibroblasts, although plasma membrane caveolae cholesterol levels in these cells are also decreased is currently under investigation. It is possible, as suggested by recent studies, that additional

plasma membrane domains besides caveolae are cholesterol-deficient in $NPC^{-/-}$ cells and therefore involved in the disease process (73).

In conclusion, the results from this report suggest that NPC1 regulates the transport of cholesterol to caveolin-1 and caveolin-2 compartments such as the TGN and plasma membrane caveolae. The results obtained from this study are consistent with the hypothesis that cholesterol obtained from late endosomes-lysosomes is transported to the TGN, either before or after reaching the plasma membrane, and that the TGN facilitates cholesterol transport to plasma membrane caveolae (35, 69). Although speculative, the increased expression of caveolin-1 and caveolin-2 in both $NPC^{+/-}$ and $NPC^{-/-}$ fibroblasts may represent a compensatory mechanism that is engaged to facilitate cholesterol transport to cholesterol-deficient caveolin-1 and caveolin-2 compartments due to a defect in NPC1.

This work was supported by grants from the Ara Parseghian Medical Research Foundation and the National Institutes of Health Grant DK56732. We sincerely appreciate the many helpful discussions and critical review of the manuscript provided by Peter G. Pentchev. We also express our gratitude to Jan E. Schnitzer for providing valuable insight into the isolation of plasma membrane caveolae using cationic colloidal silica technology. Most of all, we acknowledge the encouragement and excellent technical assistance provided by Ara M. Parseghian.

Manuscript received 2 January 2002.

REFERENCES

1. Pentchev, P. G., M. T. Vanier, K. Suzuki, and M. C. Patterson. 1995. Niemann-Pick disease type C: A cellular cholesterol lipidosis. *In* The Metabolic and Molecular Bases of Inherited Disease. 7th edition. C. R. Scriver, A. L. Beaudet, and W. S. Sly, editors. McGraw-Hill, New York. 2625–2639.
2. Xie, C., S. D. Turley, P. G. Pentchev, and J. M. Dietschy. 1999. Cholesterol balance and metabolism in mice with loss of function of Niemann-Pick C protein. *Am. J. Phys.* **276:** E336–E344.
3. Xie, C., S. D. Turley, and J. M. Dietschy. 1999. Cholesterol accumulation in tissues of the Niemann-pick type C mouse is determined by the rate of lipoprotein-cholesterol uptake through the coated-pit pathway in each organ. *Proc. Natl. Acad. Sci. USA.* **96:** 11992–11997.
4. Liscum, L., R. M. Ruggiero, and J. R. Faust. 1989. The intracellular transport of low density lipoprotein-derived cholesterol is defective in Niemann-Pick type C fibroblasts. *J. Cell Biol.* **108:** 1625–1636.
5. Coxey, R. A., P. G. Pentchev, G. Campbell, and E. J. Blanchette-Mackie. 1993. Differential accumulation of cholesterol in Golgi compartments of normal and Niemann-Pick type C fibroblasts incubated with LDL: a cytochemical freeze-fracture study. *J. Lipid Res.* **34:** 1165–1176.
6. Blanchette-Mackie, E. J., N. K. Dwyer, L. M. Amende, H. S. Kruth, J. D. Butler, J. Sokol, M. E. Comly, M. T. Vanier, J. T. August, R. O. Brady, and P. G. Pentchev. 1988. Type C Niemann-Pick disease: low density lipoprotein uptake is associated with premature cholesterol accumulation in the Golgi complex and excessive cholesterol storage in lysosomes. *J. Biol. Chem.* **85:** 8022–8026.
7. Lange, Y., J. Ye, and T. L. Steck. 1998. Circulation of cholesterol between lysosomes and the plasma membrane. *J. Biol. Chem.* **273:** 18915–18922.
8. Lange, Y., J. Ye, M. Rigney, and T. Steck. 2000. Cholesterol movement in Niemann-Pick type C cells and in cells treated with amphiphiles. *J. Biol. Chem.* **275:** 17468–17475.
9. Cruz, J.C., S. Sugii, C. Yu, and T. Y. Chang. 2000. Role of Niemann-Pick type C1 protein in intracellular trafficking of low density lipoprotein-derived cholesterol. *J. Biol. Chem.* **275:** 4013–4021.
10. Cruz, J. C., and T. Y. Chang. 2000. Fate of endogenously synthesized cholesterol in Niemann-Pick type C1 cells. *J. Biol. Chem.* **275:** 41309–41316.
11. Carstea, E. D., J. A. Morris, K. G. Coleman, S. K. Loftus, D. Zhang, C. Cummings, J. Gu, M. A. Rosenfeld, W. J. Pavan, D. B. Krizman, J. Nagle, M. H. Polymeropoulos, S. L. Sturley, Y. A. Ioannou, M. E. Higgins, M. Comly, A. Cooney, A. Brown, C. R. Kaneski, E. J. Blanchette-Mackie, N. K. Dwyer, E. B. Neufeld, T. Y. Chang, L. Liscum, and D. A. Tagle. 1997. Niemann-Pick C1 disease gene: homology to mediators of cholesterol homeostasis. *Science.* **277:** 228–231.
12. Watari, H., E. J. Blanchette-Mackie, N. K. Dwyer, J. M. Glick, S. Patel, E. B. Neufeld, R. O. Brady, P. G. Pentchev, and J. F. Strauss III. 1999. Niemann-Pick C1 protein: obligatory roles for N-terminal domains and lysosomal targeting in cholesterol mobilization. *Proc. Natl. Acad. Sci. USA.* **96:** 805–810.
13. Watari, H., E. J. Blanchette-Mackie, N. K. Dwyer, M. Watari, E. B. Neufeld, S. Patel, P. G. Pentchev, and J. F. Strauss III. 1999. Mutations in the leucine zipper motif and sterol-sensing domain inactivate the Niemann-Pick C1 glycoprotein. *J. Biol. Chem.* **274:** 21861–21866.
14. Davies, J. P., and Y. A. Ioannou. 2000. Topological analysis of Niemann-Pick C1 protein reveals that the membrane orientation of the putative sterol-sensing domain is identical to those of 3-hydroxy-3-methylglutaryl-CoA reductase and sterol regulatory element binding protein cleavage-activating protein. *J. Biol. Chem.* **275:** 24367–24374.
15. Watari, H., E. J. Blanchette-Mackie, N. K. Dwyer, M. Watari, C. G. Burd, S. Patel, P. G. Pentchev, and J. F. Strauss III. 2000. Determinants of NPC1 expression and action: key promoter regions, post-transcriptional control, and the importance of a "cysteine-rich" loop. *Exper. Cell Res.* **259:** 247–256.
16. Patel, S. C., S. Suresh, U. Kumar, C. Y. Hu, A. Cooney, E. J. Blanchette-Mackie, E. B. Neufeld, R. C. Patel, R. O. Brady, Y. C. Patel, P. G. Pentchev, and W. Y. Ong. 1999. Localization of Niemann-Pick C1 protein in astrocytes: implications for neuronal degeneration in Niemann- Pick type C disease. *Proc. Natl. Acad. Sci. USA.* **96:** 1657–1662.
17. Neufeld, E. B., M. Wastney, S. Patel, S. Suresh, A. M. Conney, N. K. Dwyer, C. F. Roff, K. Ohno, J. A. Morris, E. D. Carstea, J. P. Incardona, J. F. Strauss III, M. T. Vanier, M. C. Patterson, R. O. Brady, P. G. Pentchev, and E. J. Blanchette-Mackie. 1999. The Niemann-Pick C1 protein resides in a vesicular compartment linked to retrograde transport of multiple lysosomal cargo. *J. Biol. Chem.* **274:** 9627–9635.
18. Higgins, M. E., J. P. Davies, F. W. Chen, and Y. A. Ioannou. 1999. Niemann-Pick C1 is a late endosome-resident protein that transiently associates with lysosomes and the trans-Golgi network. *Mol. Genet. Metab.* **68:** 1–13.
19. Garver, W. S., R. A. Heidenreich, R. P. Erickson, M. A. Thomas, and J. M. Wilson. 2000. Localization of the murine Niemann-Pick C1 protein to two distinct intracellular compartments. *J. Lipid Res.* **41:** 673–687.
20. Zhang, M., N. K. Dwyer, E. B. Neufeld, D. C. Love, A. Cooney, M. Comly, S. Patel, H. Watari, J. F. Strauss III, P. G. Pentchev, J. A. Hanover, and E. J. Blanchette-Mackie. 2001. Sterol-modulated glycolipid sorting occurs in Niemann-Pick C1 late endosomes. *J. Biol. Chem.* **276:** 3417–3425.
21. Zhang, M., N. K. Dwyer, D. C. Love, A. Cooney, M. Comly, E. Neufeld, P. G. Pentchev, E. J. Blanchette-Mackie, and J. A. Hanover. 2001. Cessation of rapid late endosomal tubulovesicular trafficking in Niemann-Pick type C1 disease. *Proc. Natl. Acad. Sci. USA.* **98:** 4466–4471.
22. Holtta-Vuori, M., J. Maatta, O. Ullrich, E. Kuismanen, and E. Ikonen. 2000. Mobilization of late-endosomal cholesterol is inhibited by Rab guanine nucleotide dissociation inhibitor. *Curr. Biol.* **10:** 95–98.
23. Davies, J. P., F. W. Chen, and Y. A. Ioannou. 2000. Transmembrane molecular pump activity of Niemann-Pick C1 protein. *Science.* **290:** 2295–2298.
24. Garver, W. S., S. C. Hsu, R. P. Erickson, W. L. Greer, D. M. Byers, and R. A. Heidenreich. 1997. Increased expression of caveolin-1 in heterozygous Niemann-Pick type II human fibroblasts. *Biochem. Biophys. Res. Comm.* **236:** 189–193.
25. Garver, W. S., R. P. Erickson, J. M. Wilson, T. L. Colton, G. S. Hos-

sain, M. A. Kozloski, and R. A. Heidenreich. 1997. Altered expression of caveolin-1 and increased cholesterol in detergent insoluble membrane fractions from liver in mice with Niemann-Pick disease type C. *Biochem. Biophys. Acta.* **1361:** 272–280.
26. Pol, A., R. Luetterforst, M. Lindsay, S. Heino, E. Ikonen, and R. G. Parton. 2001. A caveolin dominant negative mutant associates with lipid bodies and induces intracellular cholesterol imbalance. *J. Cell Biol.* **152:** 1057–1070.
27. Glenney, J. R., Jr. 1992. The sequence of human caveolin reveals identity with VIP21, a component of transport vesicles. *FEBS Lett.* **314:** 45–48.
28. Kurzchalia, T. V., P. Dupree, R. G. Parton, R. Kellner, H. Virta, M. Lehnert, and K. Simons. 1992. VIP21, a 21-kD membrane protein is an integral component of *trans*-Golgi-network-derived transport vesicles. *J. Cell Biol.* **118:** 1003–1014.
29. Scheiffele, P., P. Verkade, A. M. Fra, H. Virta, K. Simons, and E. Ikonen. 1998. Caveolin-1 and -2 in the exocytic pathway of MDCK cells. *J. Cell Biol.* **140:** 795–806.
30. Rothberg, K. G., J. E. Heuser, W. C. Donzell, Y. Ying, J. R. Glenney, and R. G. W. Anderson. 1992. Caveolin, a protein component of caveolae membrane coats. *Cell.* **68:** 673–682.
31. Sargiacomo, M., M. Sudol, Z. Tang, and M. P. Lisanti. 1993. Signal transduction molecules and glycosylphosphatidylinositol-linked proteins form a caveolin-rich insoluble complex in MDCK cells. *J. Cell Biol.* **122:** 789–807.
32. Smart, E. J., Y. S. Ying, P. A. Conrad, and R. G. Anderson. 1994. Caveolin moves from caveolae to the Golgi apparatus in response to cholesterol oxidation. *J. Cell Biol.* **127:** 1185–1197.
33. Smart, E. J., Y. Ying, W. C. Donzell, and R. G. Anderson. 1996. A role for caveolin in transport of cholesterol from endoplasmic reticulum to plasma membrane. *J. Biol. Chem.* **271:** 29427–29435.
34. Murata, M., J. Peranen, R. Schreiner, F. Wieland, T. V. Kurzchalia, and K. Simons. 1995. VIP21/caveolin is a cholesterol-binding protein. *Proc. Natl. Acad. Sci. USA.* **92:** 10339–10343.
35. Fielding, P. E., and C. J. Fielding. 1996. Intracellular transport of low density lipoprotein derived free cholesterol begins at clathrin-coated pits and terminates at cell surface caveolae. *Biochemistry.* **35:** 14932–14938.
36. Uittenbogaard, A., Y. Ying, and E. J. Smart. 1998. Characterization of a cytosolic heat-shock protein-caveolin chaperone complex. Involvement in cholesterol trafficking. *J. Biol. Chem.* **273:** 6525–6532.
37. Chaney, L. K., and B. S. Jacobson. 1983. Coating cells with colloidal silica for high yield isolation of plasma membrane sheets and identification of transmembrane proteins. *J. Biol. Chem.* **258:** 10062–10072.
38. Schnitzer, J. E., D. P. McIntosh, A. M. Dvorak, J. Liu, and P. Oh. 1995. Separation of caveolae from associated microdomains of GPI-anchored proteins. *Science.* **269:** 1435–1439.
39. Heider, J. G., and R. L. Boyett. 1978. The picomole determination of free and total cholesterol in cells in culture. *J. Lipid Res.* **19:** 514–518.
40. Oh; P., and J. E. Schnitzer. 1999. Immunoisolation of caveolae with high affinity antibody binding to the oligomeric caveolin cage. *J. Biol. Chem.* **274:** 23144–23154.
41. Tran, N. L., R. B. Nagle, A. E. Cress, and R. L. Heimark. 1999. N-cadherin expression in human prostate carcinoma cell lines. An epithelial-mesenchymal transformation mediating adhesion with stromal cells. *Am. J. Pathol.* **155:** 787–798.
42. Bloom, G. S., and T. A. Brashear. 1989. A novel 58-kDa protein associates with the Golgi apparatus and microtubules. *J. Biol. Chem.* **264:** 16083–16092.
43. Monnat, J., E. M. Neuhaus, M. S. Pop, D. M. Ferrari, B. Kramer, and T. Soldati. 2000. Identification of a novel saturable endoplasmic reticulum localization mechanism mediated by the C-terminus of a Dictyostelium protein disulfide isomerase. *Mol. Biol. Cell.* **11:** 3469–3484.
44. Burgess, J. K., K. A. Hotchkiss, C. Suter, N. P. Dudman, J. Szollosi, C. N. Chesterman, B. H. Chong, and P. J. Hogg. 2000. Physical proximity and functional association of glycoprotein 1b alpha and protein disulfide isomerase on the platelet plasma membrane. *J. Biol. Chem.* **275:** 9758–9766.
45. Scherer, P. E., R. Y. Lewis, D. Volonte, J. A. Engelman, F. Galbiati, J. Couet, S. Kohtz, E. van Donselaar, P. Peters, and M. P. Lisanti. 1997. Cell-type and tissue-specific expression of caveolin-2. *J. Biol. Chem.* **272:** 29337–29346.
46. Liu, J., P. Oh, T. Horner, R. A. Rogers, and J. E. Schnitzer. 1997. Organized endothelial cell surface signal transduction in caveolae distinct from glycosylphosphatidylinositol-anchored protein microdomains. *J. Biol. Chem.* **272:** 7211–7222.
47. Kruth, H. S., M. E. Comly, J. D. Butler, M. T. Vanier, J. K. Fink, D. A. Wenger, S. Patel, and P. G. Pentchev. 1986. Type C Niemann-Pick disease. Abnormal metabolism of low density lipoprotein in homozygous and heterozygous fibroblasts. *J. Biol. Chem.* **261:** 16769–16774.
48. Koike, T., G. Ishida, M. Taniguchi, K. Higaki, Y. Ayaki, M. Saito, Y. Sakakihara, M. Iwamori, and K. Ohno. 1998. Decreased membrane fluidity and unsaturated fatty acids in Niemann-Pick disease type C fibroblasts. *Biochem. Biophys. Acta.* **1406:** 327–335.
49. Lange, Y., M. H. Swaisgood, B. V. Ramos, and T. L. Steck. 1989. Plasma membranes contain half the phospholipid and 90% of the cholesterol and sphingomyelin in cultured human fibroblasts. *J. Biol. Chem.* **264:** 3786–3793.
50. Furuchi, T., and R. G. W. Anderson. 1998. Cholesterol depletion of caveolae causes hyperactivation of extracellular signal-related kinase (ERK). *J. Biol. Chem.* **273:** 21099–21104.
51. Dupree, P., R. G. Parton, G. Raposo, T. V. Kurzchalia, and K. Simons. 1993. Caveolae and sorting in the trans-Golgi network of epithelial cells. *EMBO J.* **12:** 1597–1605.
52. Ostermeyer, A. G., J. M. Paci, Y. Zeng, D. M. Lublin, S. Munro, and D. A. Brown. 2001. Accumulation of caveolin in the endoplasmic reticulum redirects the protein to lipid storage droplets. *J. Cell Biol.* **152:** 1071–1078.
53. Sokol, J., E. J. Blanchette-Mackie, H. S. Kruth, N. K. Dwyer, L. M. Amende, J. D. Butler, E. Robinson, S. Patel, R. O. Brady, M. Comly, M. T. Vanier, and P. G. Pentchev. 1986. Type C Niemann-Pick disease: lysosomal accumulation and defective intracellular mobilization of low density lipoprotein cholesterol. *J. Biol. Chem.* **263:** 3411–3417.
54. Lusa, S., T. S. Blom, E. Eskelinen, E. Kuismanen, J. Mansson, K. Simons, and E. Ikonen. 2001. Depletion of rafts in late endocytic membranes is controlled by NPC1-dependent recycling of cholesterol to the plasma membrane. *J. Cell Sci.* **114:** 1893–1900.
55. Neufeld, E. B., A. M. Cooney, J. Pitha, E. A. Dawidowicz, N. K. Dwyer, P. G. Pentchev, and E. J. Blanchette-Mackie. 1996. Intracellular trafficking of cholesterol monitored with a cyclodextrin. *J. Biol. Chem.* **271:** 21604–21613.
56. Underwood, K. W., N. L. Jacobs, A. Howley, and L. Liscum. 1998. Evidence for a cholesterol transport pathway from lysosomes to endoplasmic reticulum that is independent of the plasma membrane. *J. Biol. Chem.* **273:** 4266–4274.
57. Garver, W. S., G. S. Hossain, M. M. Winscott, and R. A. Heidenreich. 1999. The Npc1 mutation causes an altered expression of caveolin-1, annexin II and protein kinases and phosphorylation of caveolin-1 and annexin II in murine livers. *Biochem. Biophys. Acta.* **1453:** 193–206.
58. Fielding, C. J., A. Bist, and P. E. Fielding. 1997. Caveolin mRNA levels are up-regulated by free cholesterol and down-regulated by oxysterols in fibroblast monolayers. *Proc. Natl. Acad. Sci. USA.* **94:** 3753–3758.
59. Hailstones, D., L. S. Sleer, R. G. Parton, and K. K. Stanley. 1998. Regulation of caveolin and caveolae by cholesterol in MDCK cells. *J. Lipid Res.* **39:** 369–379.
60. Bist, A., P. E. Fielding, and C. J. Fielding. 1997. Two sterol regulatory element-like sequences mediate up-regulation of caveolin gene transcription in response to low density lipoprotein free cholesterol. *Proc. Natl. Acad. Sci. USA.* **94:** 10693–10698.
61. Nohturfft, A., R. A. DeBose-Boyd, S. Scheek, J. L. Goldstein, and M. S. Brown. 1999. Sterols regulate cycling of SREBP cleavage-activating protein (SCAP) between endoplasmic reticulum and Golgi. *Proc. Natl. Acad. Sci. USA.* **96:** 11235–11240.
62. Nohturfft, A., D. Yabe, J. L. Goldstein, M. S. Brown, and P. J. Espenshade. 2000. Regulated step in cholesterol feedback localized to budding of SCAP from ER membranes. *Cell.* **102:** 315–323.
63. Orci, L., R. Montesano, P. Meda, F. Malaisse-Lagae, D. Brown, A. Perrelet, and P. Vassalli. 1981. Heterogenous distribution of filipin-cholesterol complexes across the cisternae of the Golgi apparatus. *Proc. Natl. Acad. Sci. USA.* **78:** 293–297.
64. Anderson, R. G., and R. K. Pathak. 1985. Vesicles and cisternae in the trans Golgi apparatus of human fibroblasts are acidic compartments. *Cell.* **40:** 635–643.
65. Heino, S., S. Lusa, P. Somerharju, C. Ehnholm, V. M. Olkkonen, and E. Ikonen. 2000. Dissecting the role of the golgi complex and lipid rafts in biosynthetic transport of cholesterol to the cell surface. *Proc. Natl. Acad. Sci. USA.* **97:** 8375–8380.

66. Mendez, A. J. 1995. Monensin and brefeldin A inhibit high density lipoprotein-mediated cholesterol efflux from cholesterol-enriched cells. Implications for intracellular cholesterol transport. *J. Biol. Chem.* **270:** 5891–5900.
67. Mendez, A. J., and L. Uint. 1996. Apolipoprotein-mediated cellular cholesterol and phospholipid efflux depend on a functional Golgi apparatus. *J. Lipid Res.* **37:** 2510–2524.
68. Keller, P., and K. Simons. 1998. Cholesterol is required for surface transport of influenza virus hemagglutinin. *J. Biol. Chem.* **140:** 1357–1367.
69. Wang, Y., C. Thiele, and W. B. Huttner. 2000. Cholesterol is required for the formation of regulated and constitutive secretory vesicles from the trans-Golgi network. *Traffic.* **1:** 952–962.
70. Ikonen, E., M. Tagaya, O. Ullrich, C. Montecucco, and K. Simons. 1995. Different requirements for NSF, SNAP, and Rab proteins in apical and basolateral transport in MDCK cells. *Cell.* **81:** 571–580.
71. Chang, W., K. G. Rothberg, B. A. Kamen, and R. G. W. Anderson. 1992. Lowering the cholesterol content of MA104 cells inhibits receptor-mediated transport of folate. *J. Cell Biol.* **118:** 63–69.
72. Sawamura, N., J. S. Gong, W. S. Garver, R. A. Heidenreich, H. Ninomiya, K. Ohno, K. Yanagisawa, and M. Michikawa. 2001. Site-specific phosphorylation of tau accompanied by activation of mitogen-activated protein kinase (MAPK) in brains of Niemann-Pick type C mice. *J. Biol. Chem.* **276:** 10314–10319.
73. Kruth, H. S., I. Ifrim, J. Chang, L. Addadi, D. Perl-Treves, and W. Y. Zhang. 2001. Monoclonal antibody detection of plasma membrane cholesterol microdomains responsive to cholesterol trafficking. *J. Lipid Res.* **42:** 1492–1500.

Available online at www.sciencedirect.com
SCIENCE DIRECT®
Neurochemistry International 45 (2004) 23–30
NEUROCHEMISTRY International
www.elsevier.com/locate/neuint

Fibroblast growth factor 1 is produced prior to apolipoprotein E in the astrocytes after cryo-injury of mouse brain

Toyohiro Tada[a], Jin-ichi Ito[b], Michiyo Asai[b], Shinji Yokoyama[b,*]

[a] *Department of Pathology, Nagoya City University School of Nursing, Nagoya 467-8601, Japan*
[b] *Biochemistry, Cell Biology and Metabolism, Nagoya City University Graduate School of Medical Sciences, Nagoya 467-8601, Japan*

Received 16 June 2003; received in revised form 5 August 2003; accepted 14 January 2004

Abstract

We recently reported that fibroblast growth factor 1 (FGF-1) upregulates apolipoprotein E (apoE) synthesis and its secretion as high density lipoprotein (HDL) in cultured astrocytes potentially by an autocrine or paracrine mechanism [Biochim. Biopys. Acta 1589 (2002) 261]. In order to examine pathophysiological relevance of this reaction, we studied association of the production of FGF-1 and apoE in the post-injury mouse brain. After the spot-injury of the brain by liquid nitrogen, the surface size of the wound shrunk more rapidly in the C57BL/6 wild-type mice than the apoE-knock out C57BL/6 mice. Immunohistochemical analysis of the lesions revealed that production of FGF-1 was identified in the reactive astrocytes by the day 2 after the injury in both types of mouse, prior to the production of apoE confirmed by the day 4 in the wild-type. These findings were consistent with our in-vitro observations and hypothesis that FGF-1 upregulates apoE synthesis and subsequently HDL production in the reactive astrocytes by an autocrine or paracrine manner. FGF-1 thus would exert its effect after the CNS damage through apoE secretion.

Keywords: FGF-1; Acidic FGF; ApoE; Astrocytes; Brain injury; HDL

1. Introduction

Fibroblast growth factor 1 (FGF-1, alternatively named as acidic FGF) is a potent mitogen and growth stimulation in glial cells, as well as other growth factors including FGF-2 (Engele and Bohn, 1992; Neary et al., 1994; Ryken et al., 1992; Scherer and Schnitzer, 1994; Shao et al., 1994; Thorns et al., 2001). However, its specific function in the central nervous system (CNS) has not been well established. We recently demonstrated that this factor is produced and released by the cultured rat brain cells under a certain condition and upregulates the synthesis of apolipoprotein E (apoE) and its secretion as high density lipoprotein (HDL) by the astrocyte, potentially by an autocrine or paracrine mechanism (Ueno et al., 2002). ApoE is a major apolipoprotein in cerebrospinal fluid, synthesized by astrocytes and microglias and secreted as HDL with cellular phospholipid and cholesterol (Borghini et al., 1995; Ito et al., 1999; Nakai et al., 1996; Pitas et al., 1987). Synthesis of apoE by astrocytes largely depends on the stage of cellular differentiation, and it reportedly increases during the CNS development and after cerebral injury (Aoki et al., 2003; Graham et al., 1999; Zhang et al., 2000). Therefore, apoE is thought to play key roles in maintaining the integrity of the CNS and regeneration of the nervous system by mediating the intercellular lipid transport in CNS. It is thus of importance to identify specific factors and conditions to stimulate apoE-HDL production by astrocytes as well as a specific source of such factors, especially in vivo. FGF-1 can be one of the potential candidate factors to up-regulate apoE production in pathological conditions of the brain.

In order to examine the pathophysiological relevance of the stimulation by FGF-1 of apoE-HDL synthesis in astrocytes, we undertook the in vivo study to examine expression of FGF-1 and apoE in the mouse brain of the post-injury stage. Healing of the cryo-injury was retarded in the apoE-deficient mice. FGF-1 appeared in the astrocytes of the peri-injury regions in both wild-type and apoE-deficient mice at the timing prior to the increase of apoE production in the astrocytes of the wild-type mice.

* Corresponding author. Tel.: +81-52-853-8139; fax: +81-52-841-3480.
E-mail address: syokoyam@med.nagoya-cu.ac.jp (S. Yokoyama).

0197-0186/$ – see front matter © 2004 Elsevier Ltd. All rights reserved.
doi:10.1016/j.neuint.2004.01.002

2. Materials and methods

2.1. Animals

The C57BL/6 wild-type mice (13 weeks old) were obtained from a local experimental animal supplier, and apoE knock-out C57BL/6 mice (13 weeks old) were purchased from Taconic/IBL (Germantown, NY/Fujioka, Japan). The animals were anesthetized with ether vapor. The head skin was cut open, and frostbite injury of the right hemisphere of the brain was achieved by 30 s-application of cotton applicator (1 mm diameter) dipped in liquid nitrogen to the surface of the surgically exposed skull bone overlying the right frontparietal brain. After the procedure, the brain was removed at day 2, day 4, 1-, 2- and 4-week. For evaluation of the wound healing, the size of the wound was measured on the surface of the brain at the days 2, 14 (2 weeks) and 28 (4 weeks) after the injury. The experimental procedure had been approved by the animal experiment and welfare committee of Nagoya City University Graduate School of Medical Sciences.

2.2. Immunohistochemical analysis

For histochemical studies, the frontal lobe containing the injury lesion were sliced in a thickness of 2–3 mm, and the tissue was fixed in methanol-Carnoy fixative (60% methanol, 30% chloroform, and 10% glacial acetic acid) (Gown and Vogel, 1984) for 3 h, embedded in paraffin, and sectioned for immunochemical staining. Paraffin sections were serially cut at every 3 μm and deparaffinized with xylene. After washing with phosphate buffered saline (PBS), the sections for immunochemical staining were treated with 0.3% (v/v) hydrogen peroxide in methanol for 30 min to inactivate endogenous peroxidase. Primary antibodies employed were goat anti-FGF-1, anti-apoE, and anti-glial fibrillary acidic protein (GFAP), all from Santa Cruz Biotechnology (Santa Cruz, CA). Control sections were treated with non-immunized goat immunoglobulin (Santa Cruz Biotechnology). The sections were rinsed and incubated sequentially with secondary antibody (rabbit biotinylated anti-goat immunoglobulin antibody from DAKO A/S, Glostrup. Denmark) and labeled streptavidin–biotin–peroxidase complex (Nichirei, Tokyo). After the sections were washed with PBS, the peroxidase reaction was developed in order to visualize the location of respective antigen protein by incubation in 0.02% (w/v) 3,3′-diaminobenzidine tetrahydrochloride (Sigma, St. Louis, MO) solution containing 0.003% (v/v) hydrogen peroxide and 10 mM sodium azide. Hematoxylin was used as a counter stain.

Double staining by using an immunofluorescence method was carried out for paraffin-embedded brain sections of the wild-type mice at 4-day survival periods after frostbite injury. The specimens were deparaffinized and incubated overnight with a mixture of primary antibodies including goat anti-apoE and rabbit anti-GFAP (Santa Cruz Biotechnology), followed in sequence by a 30 min incubation with Alexa Fluor 594 donkey anti-goat-IgG (H + L) (Molecular Probes, Inc., Eugene, OR, USA), washing with PBS, a 30 min incubation with Alexa Fluor 488 goat anti-rabbit-IgG (H + L) (Molecular Probes), washing with PBS, and being mounted in glycerol. Control sections were treated with a mixture of non-immune goat and rabbit immunoglobulins (Santa Cruz Biotechnology), instead of the primary antibodies. Sections were observed by laser scanning confocal microscopy (LSM5, Zeiss, Jena, Germany). Green and red channel images were merged.

3. Results

3.1. Apparent healing of the wound

After the liquid nitrogen treatment, the apparent surface size of the frostbite wound was examined at days 2, 14 (2 weeks) and 28 (4 weeks). Fig. 1A shows the brain

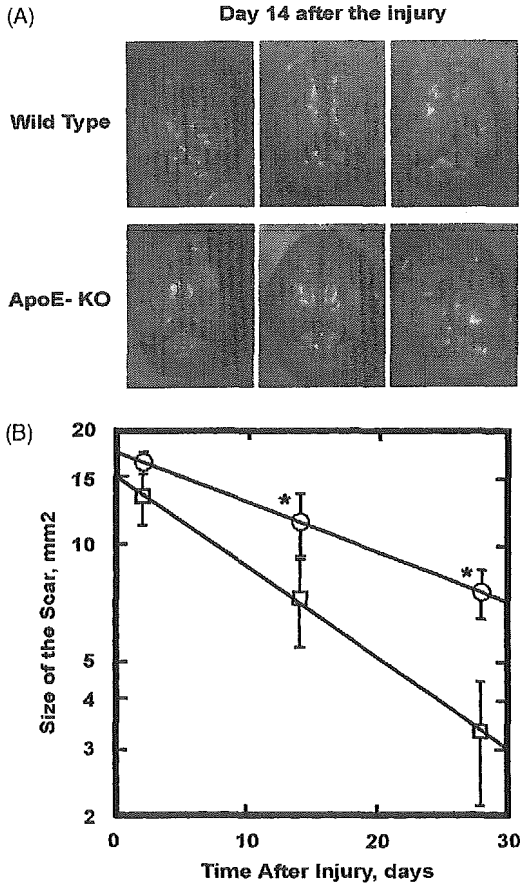

Fig. 1. (A) Mouse brains 2 weeks after the cryo-injury by liquid nitrogen on the right hemisphere. (B) The size of the injury scar on the surface of the mouse brain. The values represent the products of sagittal and cross-diameters of the scar on the brain surface (mm^2) at the days of 2, 2 weeks and 4 weeks after the injury (mean ± S.E. of three mice for each). Squares represent wild-type C57BL/6 mice and circles represent the apoE-deficient mice. Solid lines represent least square regression in semilogarithmic plots ($y = 15.1\exp(-0.023x)$ and $y = 17.3\exp(-0.013x)$. Asterisks indicate the difference by $P < 0.01$.

surface at the day 14 after the injury. The apparent size of the wounds of the wild-type mice was apparently smaller than that of the apoE-deficient mice. The size of the wound was measured and plotted in Fig. 1B. The results demonstrated that the healing process was exponential, and retarded in the apoE-deficient mice (−0.023 versus −0.013 as the slope of semilogarithmic plot). Thus, an active role of apoE was evident in the long-term

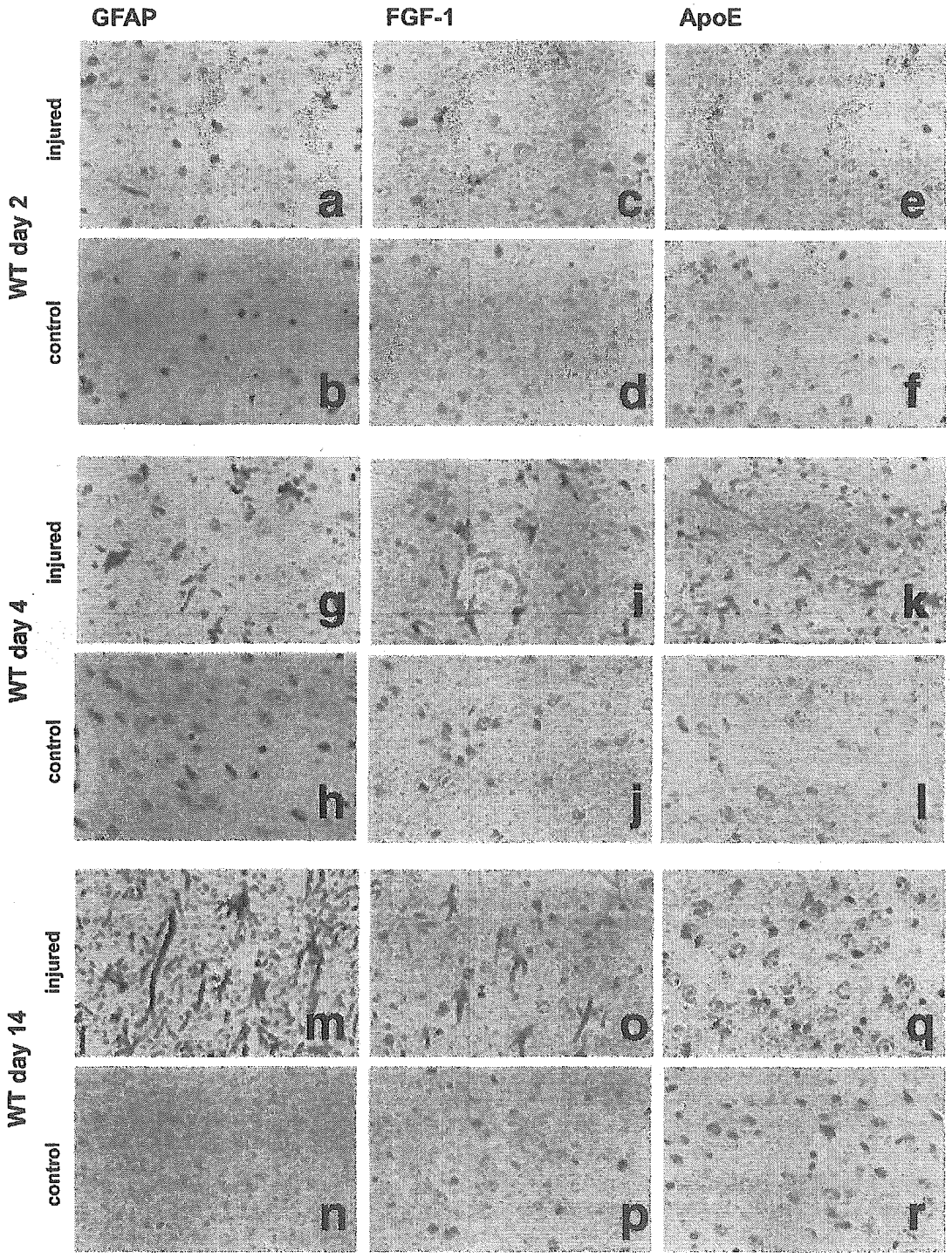

Fig. 2. Immunohistochemical analyses of GFAP, FGF-1, and apoE expression in foci of gliosis induced by frostbite-injury of the brain of the wild-type mice, at the days 2, 4, and at the day of 2 weeks after the injury. GFAP and FGF-1 were both positive in the astrocytes in the areas of gliosis in the frostbite-injured hemispheres (a, c, g, i, m and o), but neither was detected in the corresponding site of the uninjured hemisphere of the respective brain throughout the period (b, d, h, i, n and p). ApoE was not detected in the injured tissues at the day 2, appeared evidently in the astrocytes in gliosis at the day 4 (k), and was faintly demonstrated at the day of 2 weeks (q). ApoE was not detected in the counterpart of the uninjured hemisphere throughout the period (f, i and r). A scale bar indicates 1 μm.

recovery of the brain from this particular type of the injury.

In the initial recovery period, the surface of the frostbite wound of the cerebral cortex of the right lobe was slightly elevated and softened at the day 2, and tan-colored necrosis of the lesion became evident at the day 4 in both wild-type and apoE-deficient mice. Histological finding in this stage was that a cone-shaped necrotic lesion was extended from the leptomeninges to the white matter right below the cortex containing densely packed cell-debris and macrophages. At the outer margin of the wounds, small blood-vessels including dilated capillaries were evident. The necrotic tissue was

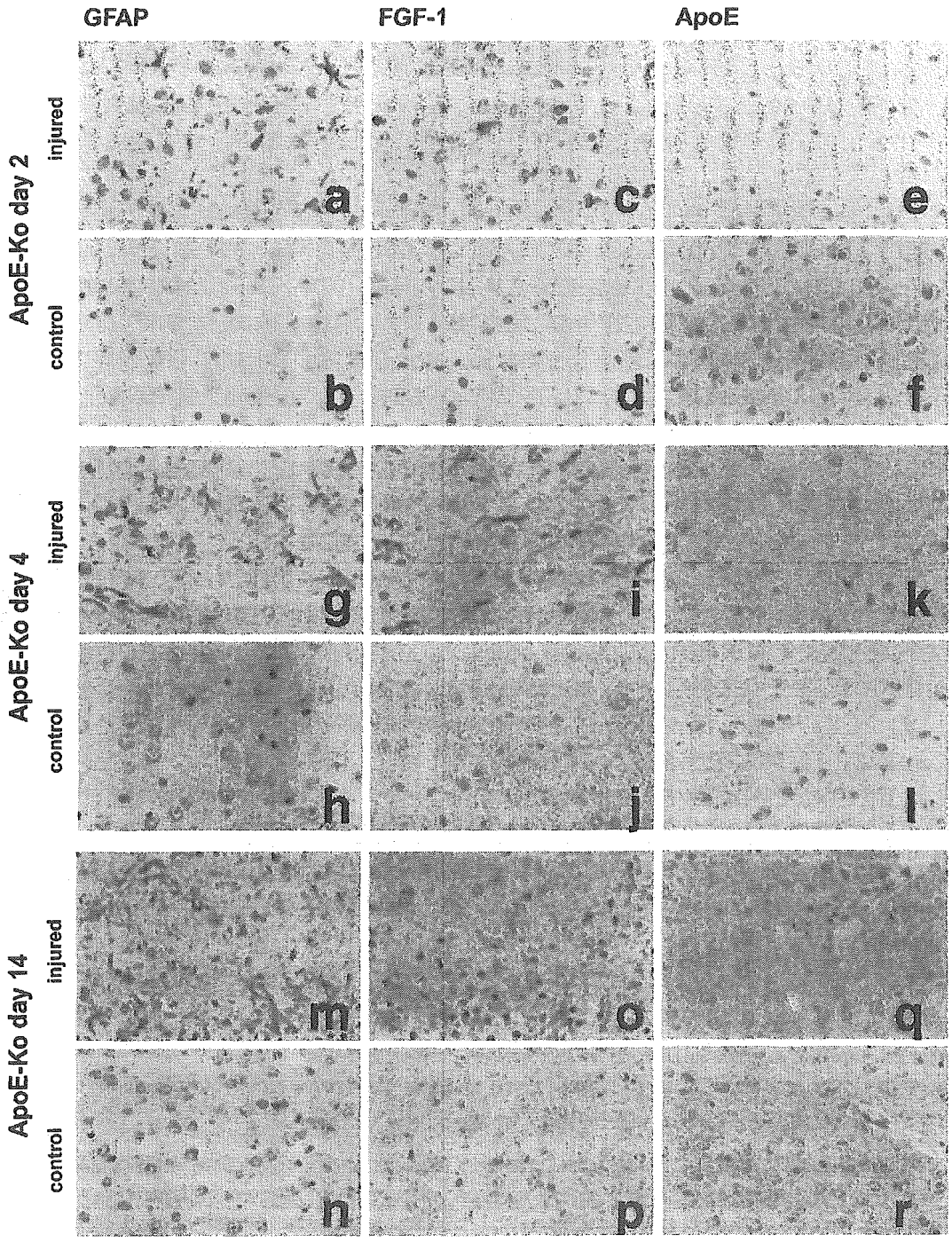

Fig. 3. Immunohistochemical analyses of GFAP, FGF-1, and apoE expression in foci of gliosis induced by frostbite-injury of the brain of the apoE-deficient mice, at the day 2, 4, and the day of 2 weeks after the injury. GFAP and FGF-1 were both positive in the astrocytes in the areas of gliosis in the frostbite-injured hemispheres (a, c, g, i, m and o), but neither was detected in the corresponding site of the uninjured hemisphere of the respective brain throughout the period (b, d, h, i, n and p), being similar to the findings in the wild-type mice shown in Fig. 3. No apoE was detected in any sites of the brain at the any timing after the injury (e, f, k, l, q and r). A scale bar indicates 1 μm.

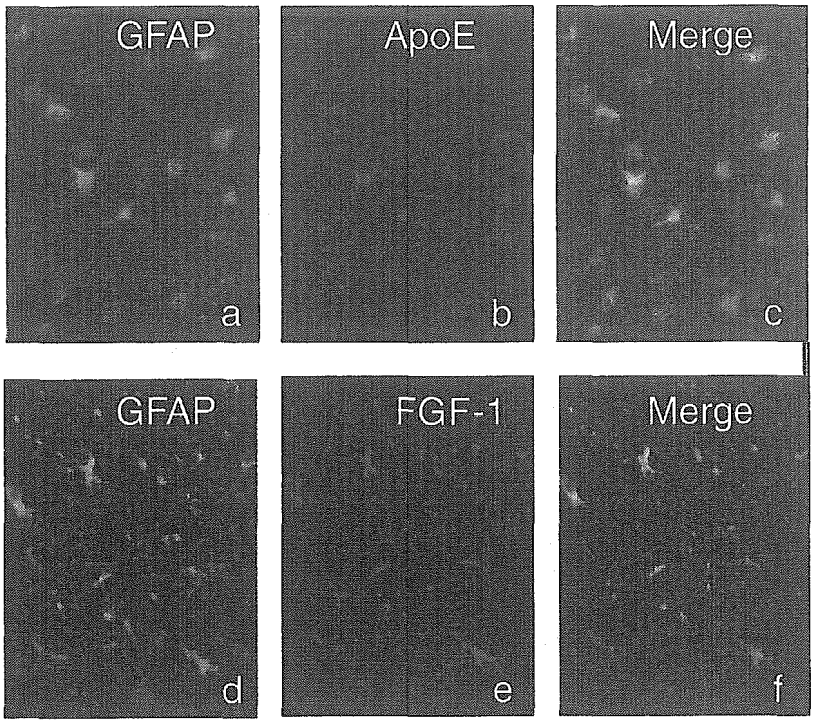

Fig. 4. Double staining of the mouse brain by using an immunofluorescence method for GFAP, apoE and FGF-1. Samples were obtained from the same brain specimens of the wild-type mice used in Fig. 2, cerebral cortex close to the frostbitten tissue. GFAP-positive (a) cells were also positive for apoE-immunostaining (b), which was verified by merging (c). GFAP-positive cells (d) and FGP-1-positive cells (e) were also shown to be identical (f).

almost completely replaced by granulation tissue composed mainly of fibroblast-like spindle cells and macrophages by the end of the second week.

3.2. Production of FGF-1 and apoE in astrocytes

The results of immunohistochemical analysis are shown in Figs. 2 and 3. At the day 2 after the injury, some astrocytes in the area adjacent to the necrotic tissue showed production of GFAP and FGF-1, in a stellate appearance with long processes in the both wild-type (Fig. 2a and c) and apoE-deficient mice (Fig. 3a and c). ApoE production was not apparent in either type of mice at this stage (Figs. 2e and 3e).

At the day 4, production of GFAP and FGF-1 became more evident in many of the astrocytes in areas of gliosis surrounding the injured tissue in both wild-type and apoE-deficient mice (Figs. 2g,j and 3g,j), and these findings were maintained at the post-injury time of 2 weeks (Fig. 2m,o and 3m,o). Presence of apoE was visualized at the day 4 and it decreased at the day of 2-week after the injury in the wild-type mice (Fig. 2k and q), but not in the apoE-deficient mice as a matter of course (Fig. 3k and q).

These observations were all in the injured hemisphere and the control non-injured side did not show apparent increase of expression of any of the three proteins examined in relation to the post-injury period.

In order to confirm that both FGF-1 and apoE are produced in astrocytes in the post injury brain, double staining for GFAP and FGF-1, and for GFAP and apoE were attempted. Fig. 4 demonstrates the results in the brain of the wild-type mice, indicating that both FGF-1 and apoE are expressed in the all GFAP-positive cells in the fields.

4. Discussion

The results of the present study are summarized as below. After the cryo-injury by liquid nitrogen of the mice brain, astrocytes in the area surrounding the lesion express GFAP and FGF-1 as an initial reaction, by the day 2, no matter whether the astrocytes can produce apoE or not. By the day 4, the reactive increase of apoE synthesis was apparent in the lesion. The lack of this subsequent increase of apoE production is apparently associated with the retarded healing of the wound as it is measured as the surface size of the scar in the apoE-deficient mice.

Astrocyte is one of the major glial cells and reacts to the injury to the nervous system. The term "gliosis" is widely used to describe the astrocyte reaction to the injury characterized as the cellular hypertrophy and hyperplasia, and the increased production of GFAP, and the cells in this stage are referred as "reactive astrocytes" (Fitch and Silver, 1999). However, true mechanisms and functions of these astrocyte reactions following the CNS injury largely remains to be

clarified. A number of investigators have suggested that there are relatively small number of astrocytes proliferating being restricted to the immediate areas of wounds (Fitch and Silver, 1999).

In the present study, the production of FGF-1 was demonstrated immunohistochemically in the post-injury reactive astrocytes of mice in vivo. FGF-1 has been thought to be produced primarily in neurons in vivo (Bizon et al., 1996; Eckenstein et al., 1994; Elde et al., 1991; Hara et al., 1994; Kage et al., 2001; Kresse et al., 1995; Schnurch and Risau, 1991; Thorns et al., 2001; Wilcox and Unnerstall, 1991), though astrocytes have also been identified as its source (Alterio et al., 1988; Eckenstein et al., 1991; Faucheux et al., 1992; Kimura et al., 1994; Magnaghi et al., 2000; Tooyama et al., 1991a,b, 1993; Yasuhara et al., 1991). In the previous report, results were controversial with respect to stimulation of FGF-1 synthesis in the reactive astrocytes. Increase of the FGF-1 expression in reactive astrocytes was shown in human brain of Alzheimer's disease (Kimura et al., 1994; Tooyama et al., 1991a) and Huntington's disease (Tooyama et al., 1993), while expression of FGF-1 was reportedly negative in the astrocytes of rat brain in the repair process after cerebral infarction (Hara et al., 1994). Thus, pathophysiological relevance has remained to be addressed for our recent finding that FGF-1 stimulated rat astrocytes to increase the synthesis of apoE and apoE-HDL by a potential autocrine mechanism when the cells were prepared after a long-time primary culture.

FGF-1 is known as a potent mitogen for normal and transformed glial cells, inducing morphological differentiation of astrocytes (Engele and Bohn, 1992; Neary et al., 1994; Ryken et al., 1992; Scherer and Schnitzer, 1994; Shao et al., 1994). Protection against apoptosis and stimulation of biosynthesis of nerve growth factor in astrocytes have also been reported as effects of FGF-1 (Thorns et al., 2001). The present study demonstrated that reactive astrocytes produce FGF-1 after the cryo-injury and subsequently apoE. Such a sequential expression in vivo of FGF-1 and apoE in the post-injury reactive astrocytes is highly consistent with our in vitro finding mentioned above and would support the hypothesis that FGF-1 production is primarily stimulated in the reactive astrocytes, which subsequently induces production of apoE and release of apoE-HDL in an autocrine manner in the injured brains. Immunostaining of apoE was positive at the post-injury day 4 but reduced at the day of 2 weeks, while the influence of apoE production seems to last throughout the healing process (Figs. 1 and 3). The major effect of apoE may thus be on the initial stage of the healing, that might have the prolonged effect.

Though the function of apoE in the CNS is not fully understood, many reports indicate its importance for the recovery from the brain injury as the increase of production and secretion of apoE was observed during and after nerve degeneration in CNS or in chronic degenerative disease of the brain (Boyles et al., 1989; Graham et al., 1999). Among various factors examined for stimulation of apoE production in brain, epidermal growth factor (Baskin et al., 1997), lipopolysaccharides and NF-kappa B (Bales et al., 2000; Saura et al., 2003) were reportedly potent regulators. The present results indicated that FGF-1 would be one of the initial signals for the apoE-mediated injury repair system in CNS, with or without the co-operation of other cytokines such as epidermal growth factor (Baskin et al., 1997). FGF-1 does not have a signal sequence for secretion through the Golgi apparatus (Abraham et al., 1986; Jaye et al., 1986), so that the mechanism for FGF-1 to be released from the reactive astrocytes has yet to be clarified. Specific mechanisms may be required such as an increase of the membrane permeability or alternatively simple disruption of the membrane (Cao and Pettersson, 1993; Jackson et al., 1992).

A positive role of apoE in the CNS wound healing was demonstrated after the cerebral cryo-injury as the healing process was significantly retarded in the apoE-deficient mice being monitored by the decrease of the surface wound size. This finding is perhaps consistent with results that apoE deficiency is associated with a poor outcome from acute brain injury including intracerebral hemorrhage (Alberts et al., 1995) and cerebral ischemia (Laskowitz et al., 1998; Laskowitz et al., 1997; Sheng et al., 1999). Various mechanisms are proposed for apoE to modify the CNS response to injury in addition to its function of removing cholesterol from the lesion and providing cholesterol for regeneration of nerve cells, such as an anti-oxidative action, down regulation of the CNS inflammatory response, and immunomodulatory properties (Graham et al., 1999; Lauderback et al., 2001; Thorns and Masliah, 1999).

FGF-1 is induced in the reactive astrocytes as a response to the cryo-injury prior to the induction of apoE. Together with our previous in vitro finding that FGF-1 enhances the expression of apoE and production of apoE-HDL (Ueno et al., 2002), we hypothesize that FGF-1 stimulates apoE-HDL production in a putative autocrine manner to contributes to the wound healing. This hypothesis should further be examined by using more specific models such as the FGF-1-deficient animals (Miller et al., 2000). The mechanism for apoE-HDL to support the recovery from the cerebral injury remains to be defined.

Acknowledgements

This work was supported by Grants-in-Aid from The Ministry of Education, Culture, Science and Technology of Japan, and the Ministry of Health, Labour and Welfare of Japan.

References

Abraham, J.A., Mergia, A., Whang, J.L., Tumolo, A., Friedman, J., Hjerrild, K.A., Gospodarowicz, D., Fiddes, J.C., 1986. Nucleotide sequence of a bovine clone encoding the angiogenic protein, basic fibroblast growth factor. Science 233, 545–548.

Alberts, M.J., Graffagnino, C., McClenny, C., DeLong, D., Strittmatter, W., Saunders, A.M., Roses, A.D., 1995. ApoE genotype and survival from intracerebral hemorrhage. Lancet 346, 575.

Alterio, J., Halley, C., Brou, C., Soussi, T., Courtois, Y., Laurent, M., 1988. Characterization of a bovine acidic FGF cDNA clone and its expression in brain and retina. FEBS Lett. 242, 41–46.

Aoki, K., Uchihara, T., Sanjo, N., Nakamura, A., Ikeda, K., Tsuchiya, K., Wakayama, Y., 2003. Increased expression of neuronal apolipoprotein E in human brain with cerebral infarction. Stroke 34, 875–880.

Bales, K.R., Du, Y., Holtzman, D., Cordell, B., Paul, S.M., 2000. Neuroinflammation and Alzheimer's disease: critical roles for cytokine/Abeta-induced glial activation, NF-kappaB, and apolipoprotein E. Neurobiol. Aging 21, 427–432 (discussion 451–453).

Baskin, F., Smith, G.M., Fosmire, J.A., Rosenberg, R.N., 1997. Altered apolipoprotein E secretion in cytokine treated human astrocyte cultures. J. Neurol. Sci. 148, 15–18.

Bizon, J.L., Lauterborn, J.C., Isackson, P.J., Gall, C.M., 1996. Acidic fibroblast growth factor mRNA is expressed by basal forebrain and striatal cholinergic neurons. J. Comp. Neurol. 366, 379–389.

Borghini, I., Barja, F., Pometta, D., James, R.W., 1995. Characterizations of lipoprotein particles isolated from human cerebrospinal fluid. Biochim. Biophys. Acta 1255, 192–200.

Boyles, J.K., Zoellner, C.D., Anderson, L.J., Kosik, L.M., Pitas, R.E., Weisgraber, K.H., Hui, D.Y., Mahley, R.W., Gebicke-Haerter, P.J., Ignatius, M.J., Shooter, E.M., 1989. A role for apolipoprotein E, apolipoprotein A–I and low density lipoprotein receptors in cholesterol transport during regeneration and remyelination of the rat sciatic nerve. J. Clin. Invest. 83, 1015–1031.

Cao, Y., Pettersson, R.F., 1993. Release and subcellular localization of acidic fibroblast growth factor expressed to high levels in HeLa cells. Growth Factor 8, 277–290.

Eckenstein, F.P., Andersson, C., Kuzis, K., Woodward, W.R., 1994. Distribution of acidic and basic fibroblast growth factors in the mature, injured and developing rat nervous system. Prog. Brain Res. 103, 55–64.

Eckenstein, F.P., Shiplay, G.D., Nishi, R., 1991. Acidic and basic fibroblast growth factors in the nervous system: distribution and differential alteration of levels after injury of central versus peripheral nerve. J. Neurosci. 11, 412–419.

Elde, R., Cao, Y.H., Cintra, A., Brelje, T.C., Pelto-Huikko, M., Junttila, T., Fuxe, K., Pettersson, R.F., Hokfelt, T., 1991. Prominent expression of acidic fibroblast growth factor in motor and sensory neurons. Neuron 7, 349–364.

Engele, J., Bohn, M.C., 1992. Effects of acidic and basic fibroblast growth factors (aFGF, bFGF) on glial precursor cell proliferation: age dependency and brain region specificity. Dev. Biol. 152, 363–372.

Faucheux, B.A., Cohen, S.Y., Delaere, P., Tourbach, A., Dupuis, C., Hartmann, M.P., Jeanny, J.C., Hauw, J.J., Courtois, Y., 1992. Glial cell localization of acidic fibroblast growth factor-like immunoreactivity in the optic nerve of young adult and aged mammals. Gerontology 38, 308–314.

Fitch, M.T., Silver, J., 1999. Beyond the glial scar. Cellular and molecular mechanism by which glial cells contribute to CNS regenerative failure. In: Tuzuki, M.H., Kordower, J.H. (Eds.), CNS Regeneration: Basic Science and Clinical Advances. Academic Press, San Diego, pp. 55–88.

Gown, A.M., Vogel, A.M., 1984. Monoclonal antibodies to human intermediate filament proteins. II. Distribution of filament proteins in normal human tissues. Am. J. Pathol 114, 309–321.

Graham, D.I., Horsburgh, K., Nicoll, J.A., Trasdale, G.M., 1999. Apolipoprotein E and the response of the brain to injury. Acta Neurochirurg. Suppl. 73, 89–92.

Hara, Y., Tooyama, I., Yasuhara, O., Akiyama, H., McGeer, P.L., Handa, J., Kimura, H., 1994. Acidic fibroblast growth factor-like immunoreactivity in rat brain following cerebral infarction. Brain Res. 664, 101–107.

Ito, J., Zhang, L.-Y., Asai, M., Yokoyama, S., 1999. Differential generation of high-density lipoprotein by endogenous and exogenous apolipoproteins in cultured fetal rat astrocytes. J. Neurochem. 72, 2362–2369.

Jackson, A., Friedman, S., Zhan, X., Engleka, K.A., Forough, R., Maciag, T., 1992. Heat shock induces the release of fibroblast growth factor 1 from NIH 3T3 cells. Proc. Natl. Acad. Sci. U.S.A. 89, 10691–10695.

Jaye, M., Howk, R., Burgess, W., Ricca, G.A., Chiu, I.M., Ravera, M.W., O'Brien, S.J., Modi, W.S., Maciag, T., Drohan, W.N., 1986. Human endothelial cell growth factor: cloning. Science 233, 541–545.

Kage, M., Yang, Q., Sato, H., Matsumoto, S., Kaji, R., Akiguchi, I., Kimura, H., Tooyama, I., 2001. Acidic fibroblast growth factor (FGF-1) in the anterior horn cells of ALS and control cases. NeuroReport 12, 3799–3803.

Kimura, H., Tooyama, I., McGeer, P.L., 1994. Acidic FGF expression in the surroundings of senile plaques. Tohoku J. Exp. Med. 174, 279–293.

Kresse, A., Pettersson, R., Hokfelt, T., 1995. Distribution of acidic fibroblast growth factor mRNA-expressing neurons in the adult mouse central nervous system. J. Comp. Neurol. 359, 323–339.

Laskowitz, D.T., Sheng, H., Bart, R.D., Joyner, K.A., Roses, A.D., Warner, D.S., 1997. Apolipoprotein E-deficient mice have increased susceptibility to focal cerebral ischemia. J. Cereb. Blood Flow Metab. 17, 753–758.

Laskowitz, D.T., Horsburgh, K., Roses, A.D., 1998. Apolipoprotein E and the CNS response to injury. J. Cereb. Blood Flow Metab. 18, 465–471.

Lauderback, C.M., Hackett, J.M., Keller, J.N., Varadarajan, S., Szweda, L., Kindy, M., Markesbery, W.R., Butterfield, D.A., 2001. Vulnerability of synaptosomes from apoE knock-out mice to structural and oxidative modifications induced by Aβ(1–40): implications for Alzheimer's disease. Biochemistry 40, 2548–2554.

Magnaghi, V., Riva, M.A., Cavarretta, I., Martini, L., Melcangi, R.C., 2000. Carticosteroids regulate the gene expression of FGF-1 and FGF-2 in cultured rat astrocytes. J. Mol. Neurosci. 15, 11–18.

Miller, D.L., Ortega, S., Bashayan, O., Basch, R., Basilico, C., 2000. Compensation by fibroblast growth factor 1 (FGF-1) does not account for the mild phenotypic defects observed in FGF2 null mice. Mol. Cell Biol. 20, 2260–2268.

Nakai, M., Kawamata, T., Maeda, K., Tanaka, C., 1996. Expression of apoE mRNA in rat microglia. Neurosci. Lett. 211, 41–44.

Neary, J.T., Whittemore, S.R., Zhu, Q., Norenberg, M.D., 1994. Synergistic activation of DNA synthesis in astrocytes by fibroblast growth factors and extracellular ATP. J. Neurochem. 63, 490–494.

Pitas, R.E., Boyles, J.K., Lee, S.H., Foss, D., Mahley, R.W., 1987. Astrocytes synthesize apolipoprotein E and metabolize apolipoprotein E-containing lipoproteins. Biochim. Biophys. Acta 917, 148–161.

Ryken, T.C., Traynelis, V.C., Lim, R., 1992. Interaction of acidic fibroblast growth factor and transforming growth factor-beta in normal and transformed glia in vitro. J. Neurosurg. 76.

Saura, J., Petegnief, V., Wu, X., Liang, Y., Paul, S.M., 2003. Microglial apolipoprotein E and astroglial apolipoprotein J expression in vitro: opposite effects of lipopolysaccharide. J. Neurochem. 85, 1455–1467.

Scherer, J., Schnitzer, J., 1994. Growth factor effects on the proliferation of different retinal glial cells in vitro. Brain Res. Dev. Brain Res. 80, 209–221.

Schnurch, H., Risau, W., 1991. Differentiating and mature neurons express the acidic fibroblast growth factor gene during chick neural development. Development 111, 1143–1154.

Shao, N., Wang, H., Zhou, T., Xue, Y., Liu, C., 1994. Heparin potentiation of the effect of acidic fibroblast growth factor on astrocytes and neurons. Life Sci. 54, 785–789.

Sheng, H., Laskowitz, D.T., Mackensen, B., Kudo, M., Pearlstein, R.D., Warner, D.S., 1999. Apolipoprotein E deficiency worsens outcome from global cerebral ischemia in the mouse. Stroke 30, 1118–1124.

Thorns, V., Licastro, F., Maliah, E., 2001. Locally reduced levels of acidic FGF lead to decreased expression of 28-kDa calbindin and contribute to the selective vulnerability of the neurons in rhe entorhinal cortex in Alzheimer's disease. Neuropathology 21, 203–211.

Thorns, V., Masliah, E., 1999. Evidence for neuroprotective effects of acidic fibroblast growth factor in Alzheimer disease. J. Neuropathol. Exp. Neurol. 58, 296–306.

Tooyama, I., Akiyama, H., McGeer, P.L., Hara, Y., Yasuhara, O., Kimura, H., 1991a. Acidic fibroblast growth factor-like immunoreactivity in brain of Alzheimer patients. Neurosci. Lett. 121, 155–158.

Tooyama, I., Hara, Y., Yasuhara, O., Oomura, Y., Sasaki, K., Muto, T., Suzuki, K., Hanai, K., Kimura, H., 1991b. Production of antisera to acidic fibroblast growth factor and their application to immunohistochemical study in rat brain. Neuroscience 40, 769–779.

Tooyama, I., Kremer, H.P.H., Hayden, M.R., Kimura, H., McGeer, E.G., McGeer, P.L., 1993. Acidic and basic fibroblast growth factor-like immunoreactivity in the striatum and midbrain in Huntington's disease. Brain Res. 610, 1–7.

Ueno, S., Ito, J., Nagayasu, Y., Furukawa, T., Yokoyama, S., 2002. An acidic fibroblast growth factor-like factor secreted into brain cell culture medium upregulates apoE synthesis, HDL secretion and cholesterol metabolism in rat astrocytes. Biochim. Biophys. Acta 1589, 261–272.

Wilcox, B.J., Unnerstall, J.R., 1991. Expression of acidic fibroblast growth factor mRNA in the developing and adult rat brain. Neuron 6, 397–409.

Yasuhara, O., Tooyama, I., Akiyama, H., Akiguchi, I., Kimura, J., McGee, P.L., Hara, Y., Kimura, H., 1991. Reactive astrocytes express acidic fibroblast growth factor in Alzheimer's disease brain. Dementia 2, 64–70.

Zhang, L.-Y., Ito, J., Kato, T., Yokoyama, S., 2000. Cholesterol homeostasis in rat astrocytoma cells GA-1. J. Biochem. 128, 837–845.